I. PHOTOMETRIC DETERMINATION OF IONIZATION OF CLOUD CHAMBER TRACKS

II. CLOUD CHAMBER STUDY OF CHARGED V-PARTICLES

Thesis by

Egil Kristoffer Björnerud

In Partial Fulfillment of the Requirements

for the Degree of

Doctor of Philosophy

California Institute of Technology

Pasadena, California

1955

ACKNOWLEDGEMENTS

It is with great pleasure that I take this opportunity to express my gratitude to the Staff of the Cosmic Ray Laboratory. Throughout these experiments Drs. C. D. Anderson, R. B. Leighton and C. M. York were a constant source of inspiration. For their enthusiasm, their patience and their active participation, and for their supervision of this work, I would like to express my sincere appreciation.

I am indebted to Dr. G. Münch of the Astrophysics Department for the use of the microphotometer.

I also wish to express my gratitude to the Royal Norwegian Council for Scientific and Industrial Research for a fellowship received during the year 1952. The experimental work described in this thesis was supported in part by the joint program of the Office of Naval Research and the Atomic Energy Commission.

ABSTRACT

A photoelectric method for the measurement of ionization of cloud chamber tracks has been developed. The principal feature of the method is the use of a comparison track of known ionization in the same part of the chamber. A microphotometer slit is made to scan the track perpendicular to its direction and a tracing of the transmission of the track relative to the background transmission is obtained. A calibration curve is established and the method is used to measure the ionization of various tracks. The error of measurement is of the order of 10 per cent. A theoretical treatment of the problem is carried out to show the effects of various physical parameters not easily ascertained experimentally.

An analysis of 101 charged V-particles decays, observed with a double cloud chamber, is presented. The events in the upper chamber appear to have markedly different properties from those in the lower. The particles in the upper chamber have measured properties which are in every respect consistent with those of the kappa meson: (a) lifetime 5×10^{-10} to 2×10^{-10} sec; (b) mass $1000 m_e$, and (c) transverse momentum distribution consistent with a three-body decay scheme. The majority of the particles in the lower chamber, on the other hand, are tentatively identified as charge hyperons with the aid of two cases which appear to have proton secondaries: (a) lifetime 10^{-10} to 3×10^{-10} sec; and (b) transverse momentum distribution consistent with a two-body decay scheme.

TABLE OF CONTENTS

PART	TITLE	PAGE
I	PHOTOMETRIC DETERMINATION OF IONIZATION OF CLOUD CHAMBER TRACKS	
	1. Introduction	1
	2. Apparatus	2
	3. Theoretical Considerations	12
	4. Preliminary Measurements	20
	5. The Use of Comparison Tracks	25
	6. Correction Procedure	27
	7. Calibration	29
	8. Errors of Measurement	33
	9. Application of the Method	34
	10. Limitation of the Method	41
	11. Suggested Improvements of the Method	44
	12. List of Figures	45
	13. References	46
II	CLOUD CHAMBER STUDY OF CHARGED V-PARTICLES	
	1. Introduction	47
	2. Apparatus and Measuring Techniques	48
	3. The Data	51
	4. A Preliminary Survey of the Data	54
	4:1 Distribution of decay points	54
	4:2 Search for associated γ-rays	63
	4:3 Mechanism of production	65

TABLE OF CONTENTS (Cont'd)

PART		TITLE	PAGE
II (Cont'd)	5.	Determination of Lifetimes of Charged V-Particles	68
		5:1 Reduction of the data	69
		5:2 The upper chamber	72
		5:3 The lower chamber	82
	6.	Additional Properties of Charged V-Particles	85
		6:1 Masses of charged V-particles and their decay products	86
		6:2 The distribution of transverse momentum	89
		6:3 The distribution of momentum in the center-of-mass system	92
	7.	The Frequency of Production of Charged V-particles	94
	8.	The Charged Hyperon (V_1^+)	97
	9.	Conclusions	101
	10.	List of Figures	105
	11.	References	106

I. PHOTOMETRIC DETERMINATION OF IONIZATION OF CLOUD CHAMBER TRACKS

1. Introduction

In an analysis of cloud chamber events, which are recorded on photographic film, it is often desirable to obtain estimates of the masses of the particles involved. When the cloud chamber is operated in a magnetic field, such as in this experiment,* the momentum of a particle can be determined by measurements of the curvature of track on the film. But in order to arrive at a reasonable estimate of the mass it is also necessary to know the ionization of the particle to a fair degree of accuracy. In the past, working with the apparatus used in this experiment, ionization estimates were made visually.[1-4] The method of droplet counting, successfully used with other cloud chambers,[5,6] was not applicable. The time between the passage of the triggering particles through the chambers and the expansion was not of the length required for the ions to diffuse sufficiently far to allow the individual droplets to be resolved, since this would mean less well defined tracks and consequently inaccurate curvature measurements. However, it was hoped that improvements over the visual estimates could be made by measuring the density (or transmission) of tracks on the film by photoelectric means. This method has successfully been applied to nuclear emulsions;[7] however, there the situation is somewhat different as the grains in the emulsion are directly affected by the ionizing particles.

---

*The cloud chamber and its operation is described in Part II, Section 2.

Since the present measurements were begun, there has been a report of a similar technique used successfully on cloud chamber pictures.[8]

It must be emphasized that the method presented here is of a preliminary nature, and that several improvements and modifications can be made. A program for further development will be outlined.

2. Apparatus

The apparatus used was a precision microphotometer which was designed primarily for the measurement of spectroscopic plates. However it was easily adapted for measuring the cloud chamber films. The entire set-up is shown in Fig. 1. The film was mounted between glass plates on the carriage which could be moved in two perpendicular directions, one of which had a four-speed automatic precision drive. The film was so placed on the carriage that the track to be measured was perpendicular to the direction of this precision drive. Light from a voltage regulated projection lamp, in series with a variable rheostat, was projected onto the film (Fig. 2). The illuminated field was then magnified, and focused on the slit. A photograph of the slit and a projected track is shown in Fig. 3. The track was moved across the slit by the precision drive in the direction shown by the arrow. The light admitted by the slit was picked up by an RCA - 931A photo-tube and the out-put of the tube was amplified and fed to a Leeds and Northrup Speedomax recorder.

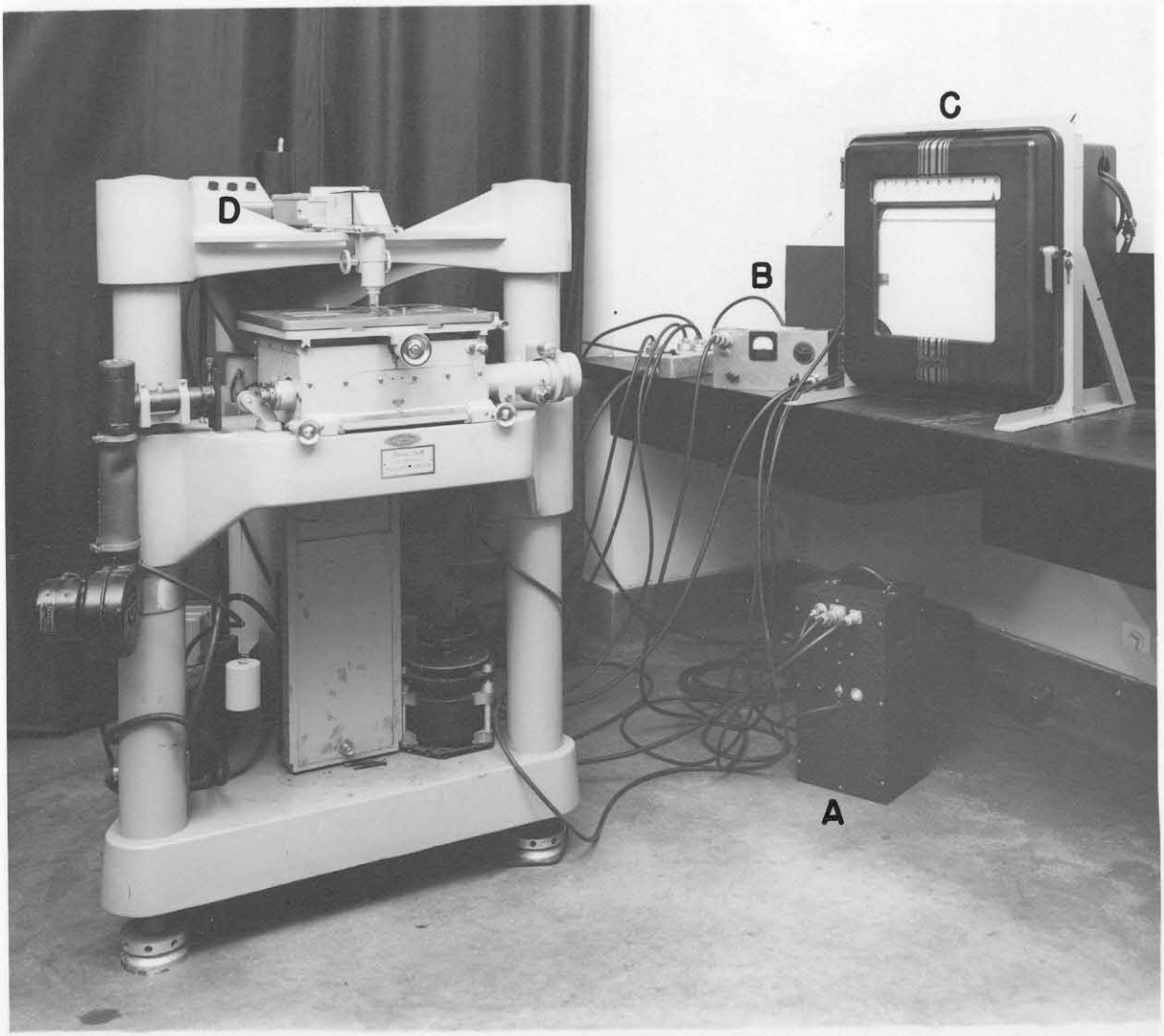

Fig. 1. The microphotometer and associated electronic apparatus. (A) the power supply and high voltage supply, (B) the amplifier, and (C) the Leeds and Northrup Speedomax recorder. The controls for the carriage movement are located at (D).

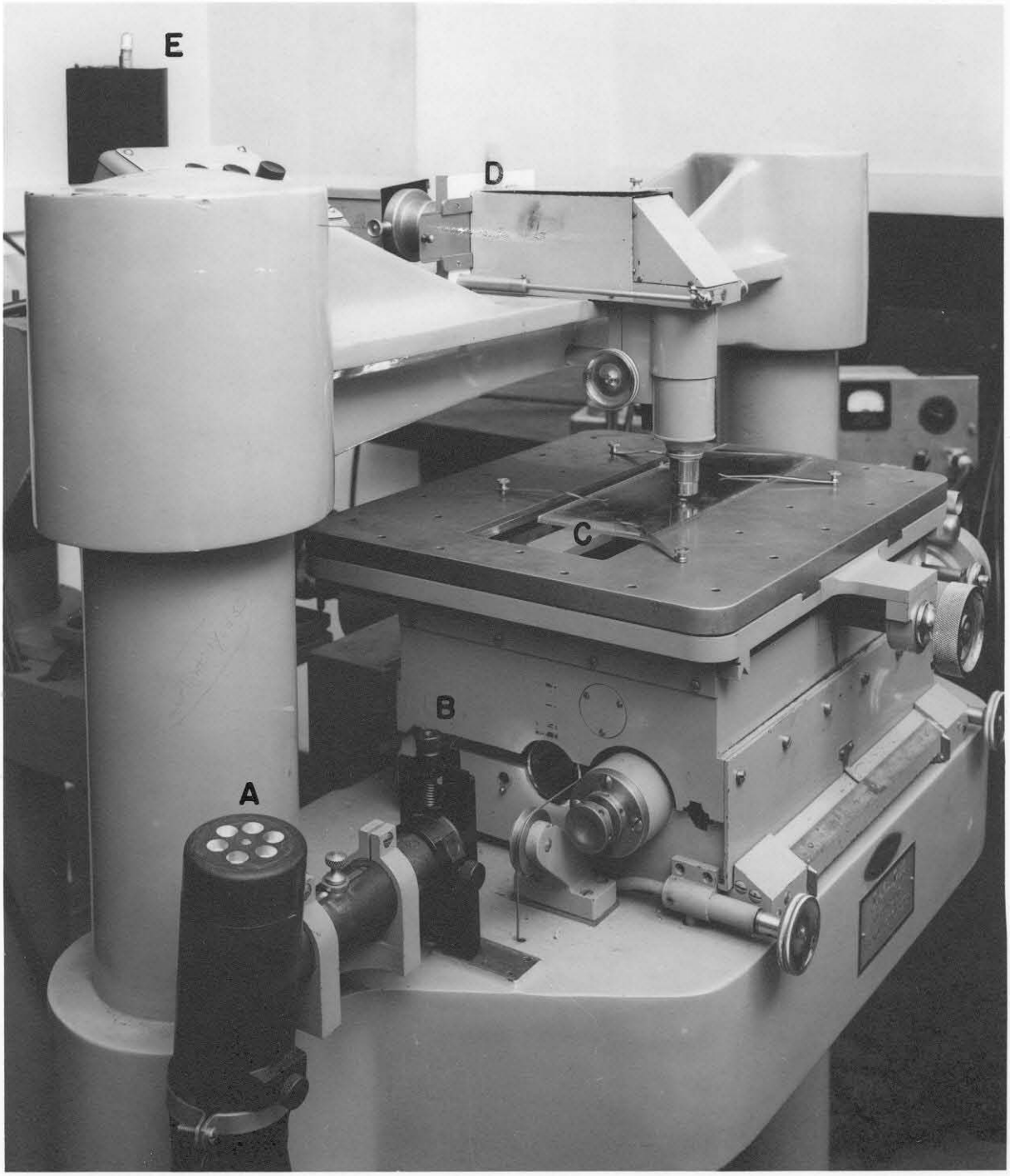

Fig. 2. A close-up view of the microphotometer. The film on the carriage (C) is illuminated by a voltage regulated projection lamp (A). A red filter and a limiting aperture (B) is inserted in the lightpath to minimize scattering effects. The microscope objective focuses the image of the track onto a slit (D), through which the light is admitted to the phototube (E).

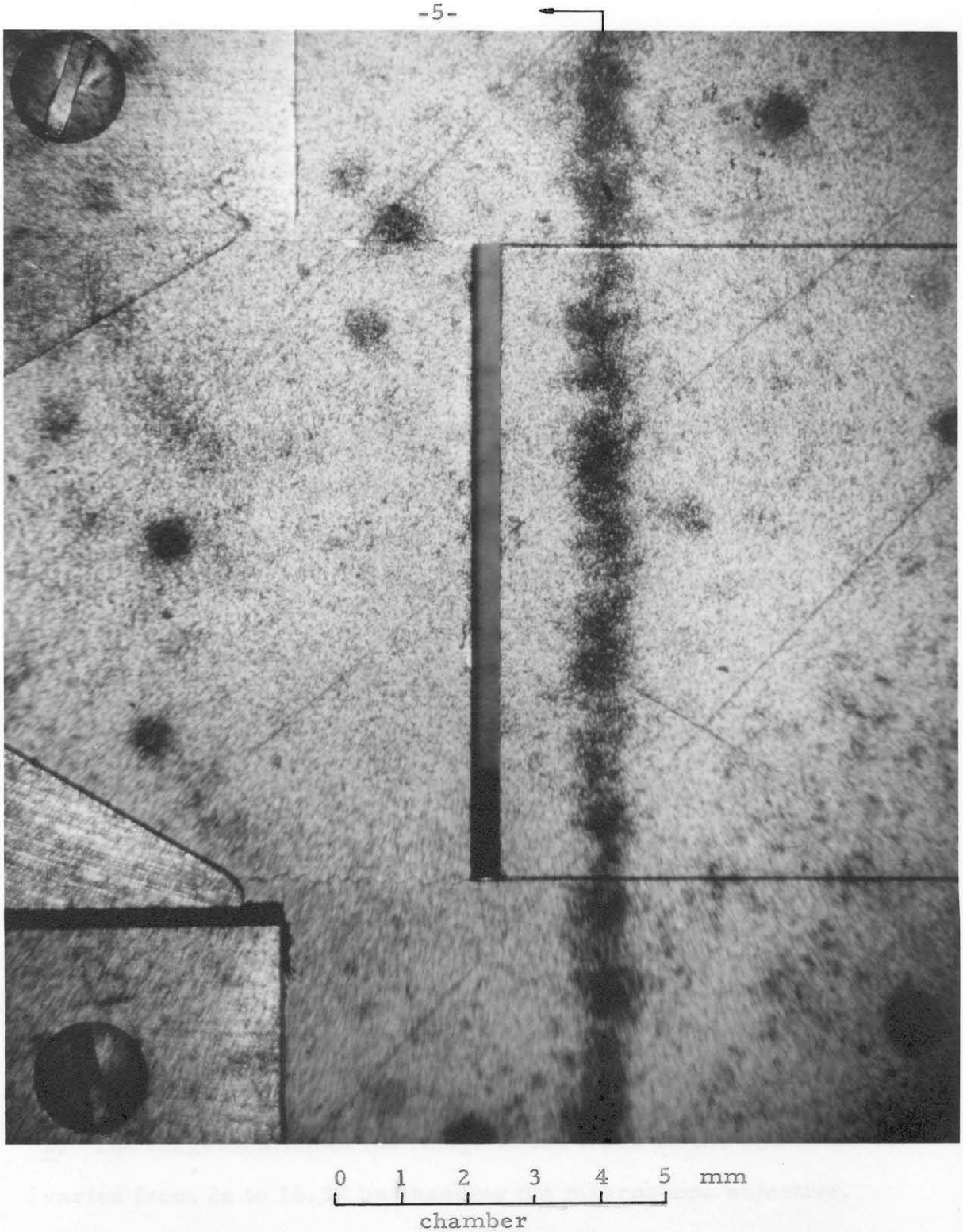

Fig. 3. The slit and the image of a heavily ionizing cloud chamber track. (enlargement 4.25 X) The total magnification from chamber to photograph is 11 times; a scale of dimensions in the chamber is shown. The instrument scans the track in the direction of the arrow.

A schematic diagram of the electronic circuit is shown in Fig. 4. The amplifier is based on the Vance-circuit[9, 10] and its principal features are: (1) very high stability, (2) extremely linear relationship between in-put and out-put, and (3) high gain. The amplifier is so designed that the gain depends only upon the ratios of the resistances of wire-wound resistors; this insures stable calibrations and linearity of scale. The amplifier is capable of measuring the out-put of the photo-tube to within a fraction of 1 per cent. A warm-up period of about one-half hour is required to insure stability.

The microphotometer was designed to measure the transmission of the part of the film projected through the slit. Several degrees of freedom, however, were available in the use of the instrument. A schematic diagram of the various adjustable parts (numbered 1 to 7) of the instrument is shown in Fig. 5. And, in order to obtain optimum reproducible conditions for the transmission measurements, these degrees of freedom had to be adjusted.

1. The out-put of the projection lamp could be adjusted with a variable rheostat. The power supplied to the lamp was chosen well below the power-rating for the lamp to insure long life, and was not changed throughout the measurements.

2. The magnification of the image of the track on the slit could be varied from 2x to 16.3x by changing the microscope objective. The magnification from chamber to film was 1/6.3x, and in order to obtain an image on the slit larger than actual size in the chamber, only one objective was used, having a magnification of 16.3x.

3. Both the length and the width of the slit could be varied. The length of the slit was found not to be very critical, however the

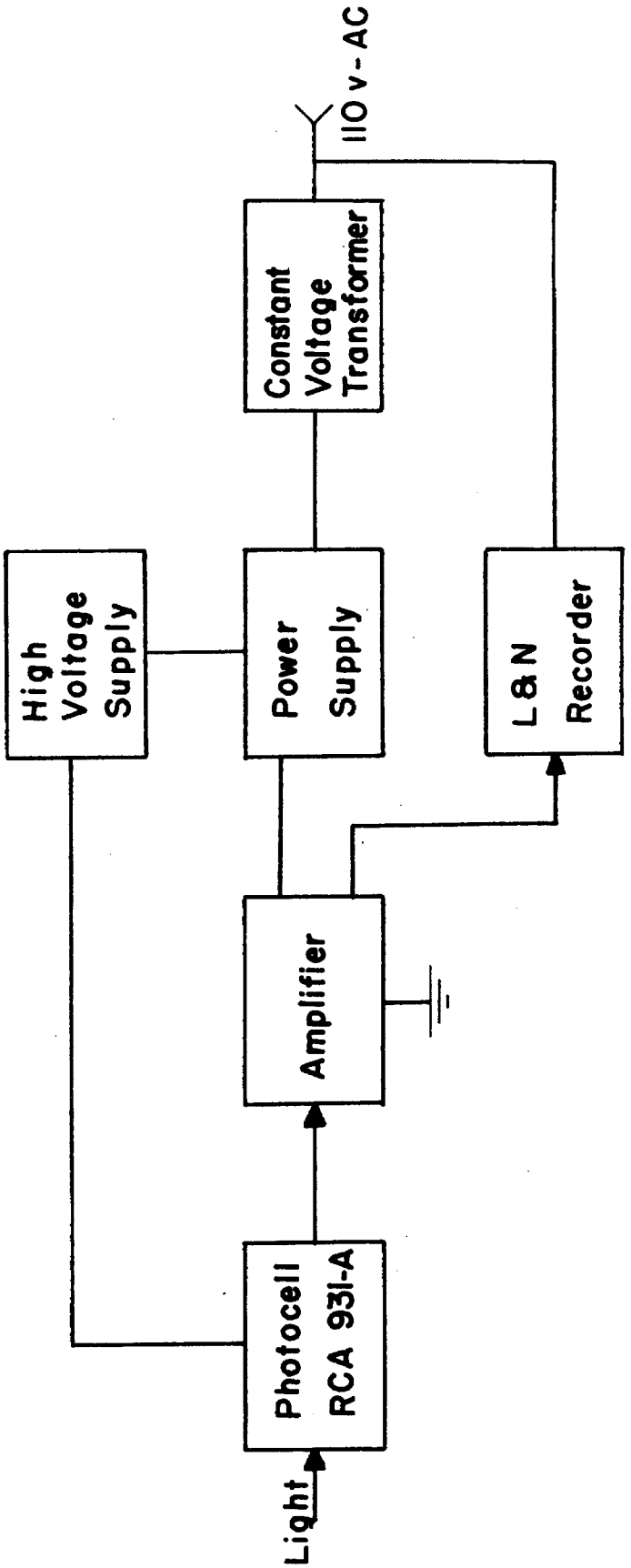

Block diagram of microphotometer circuit

Figure 4

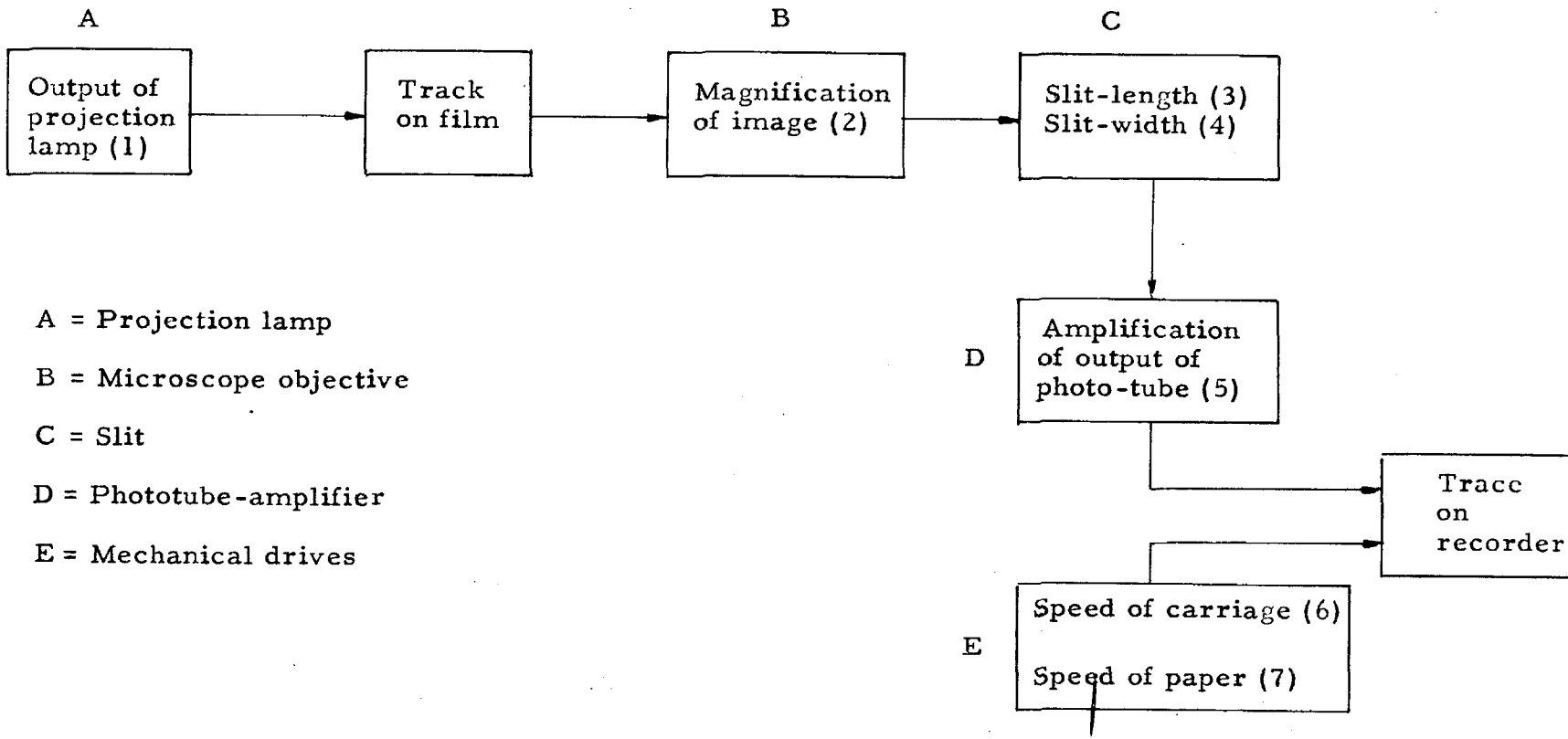

Figure 5. Schematic diagram of the degrees of freedom available in the use of the microphotometer. (Numbered from (1) to (7)).

longer the slit used the fewer measurements had to be made along the track, and also the fluctuations in density along the length of track covered by the slit would tend to average out. The maximum length of slit available was 2.50 cm ($\sim$ 1 cm in chamber), and this length was used for most of the measurements. For very curved tracks it was necessary to use a shorter slit length.

4. The width of the slit, on the other hand, was found to be very critical. Too narrow a slit would make the instrument respond to minute fluctuations in density both across the track and in the background. A very wide slit would average out the background fluctuations, but would not give a measurable response when scanning across the track. The slit-width chosen for the measurements, a compromise between these two extreme conditions, was 1.5 mm. This corresponds to 0.58 mm in the chamber, and is of the order of the track-width. Measurements on the change in transmission of a track as a function of slit-width will be discussed in Section 4.

5. The amplification of the out-put of the photo-tube could be varied by a factor of about 10^4. For each measurement the amplification was adjusted so that when the slit was scanning the background a recorder-pen deflection of approximately 0.9 (full-scale = 1.0) was obtained. The value 0.9 was chosen rather than 1.0 to allow for variation in the background transmission.

6 and 7. Both the speed of the film-holder carriage and the speed of the recorder paper were adjustable, but only within a narrow range. The carriage speed (i.e. the speed with which the track moved across the slit) was chosen so that the total scanning period, including the time it took to scan 3-4 track widths on each side of

the track, was about 15 seconds. The paper speed was adjusted to give a linear scale of 54 times that of the film, or 3.3 times that of the slit. This magnification was found to give a trace which was easy to read and at the same time occupied very little space.

It is essential for these measurements that the recorder-galvanometer reading is proportional to the amount of light reaching the photo-tube; and in order to test this, the following experiment was performed: A calibrated step wedge, with very uniform density for each step was placed under the microscope in the usual manner. For each step the slit-widths corresponding to galvanometer readings of .9, .7, .5, .3, and .1 were noted. Similar sets of readings were taken for a total of nine steps, varying in transmission factors from 87.0 per cent to 6.5 per cent, covering the range of film blackening encountered on the cloud chamber photographs.

Since the amount of light admitted to the photo-tube through the slit is directly proportional to the width of the slit, the ratio of the galvanometer readings should be the same as the ratio of the corresponding slit-width if the instrument is strictly linear in its response. The results obtained as described in Table I show that this holds true.

In the table the galvanometer-reading ratios are shown in the left-hand column, and are constant for the nine steps. All slit widths ratios were taken with respect to the slit width corresponding to the galvanometer reading of .9. The percent transmission values for each step of the wedge are also shown.

Step no	0	1	2	3	4	5	6	7	8
o/oT									
galv. ratio	87.0	68.3	51.9	38.2	27.3	19.5	13.4	9.1	6.5
.778	.791	.762	.778	.775	.776	.778	.776	.771	.770
.556	.627	.550	.556	.550	.554	.561	.554	.555	.550
.331	.308	.337	.333	.325	.333	.333	.336	.337	.328
.111	.08	.09	.087	.099	.112	.114	.111	.111	.117

Table I. Linearity test of microphotometer. For each of nine steps (0-8) of a calibrated step-wedge (ranging in transmission from 87.0 to 6.5°/o) a set of slit-width and galvanometer readings were taken. By varying the slit-widths, the galvanometer was set to read .9, .7, .5, .3, and .1 for each step. The ratio of these galvanometer settings (i.e. $\frac{.7}{.9}$, $\frac{.5}{.9}$, $\frac{.3}{.9}$ and $\frac{.1}{.9}$, constant for each step) are shown in the left-hand column. The corresponding ratios of the slit-widths (each with respect to the value at the galvanometer setting of .9) are shown in the vertical columns, beginning with step no. 0.

3. Theoretical Considerations

The method adopted for the measurement of the selected density-dependent parameter and its correlation with ionization was arrived at by an empirical approach. However, it is very instructive to investigate the problem from a theoretical point of view before describing the method in detail.

The physical process under consideration can briefly be described: a charged particle passing through the chamber triggers the counter banks; and after a time delay τ , during which time the ions formed along the path of the particle will have diffused away from their point of formation, the chamber is expanded and supersaturation takes place. The ions are now covered with water-forming drops and their mobility is reduced to zero. A photograph of these tracks, properly illuminated, is taken, and after processing the film, the images of the droplets along the track are projected onto the slit of the microphotometer and the transmission of the film is measured. It is desired to find a relation between the transmission and the number of ions per unit length along the track.

If recombination of the ions formed along the path of the particle is neglected, the distribution of ions at a distance r from the center of the track, after a time τ , is given by:[11]

$$N(r) = \frac{n}{4\pi D\tau} \exp\left(-r^2/4D\tau\right) \qquad (1)$$

where n is the total number of ions per unit length of track, and D is the diffusion coefficient of the ions. The projected distribution on the plane of the film of the droplets formed on these ions is found by integration:

$$\rho(x)dx = \frac{ne}{4\pi D\tau}\left\{ \int_{-\infty}^{\infty} \exp-\left[(x^2+y^2)/4D\tau\right] \; dy \right\} dx$$

$$\rho(x)dx = \frac{ne}{\sqrt{4\pi D\tau}} \exp\left(-x^2/4D\tau\right)dx \qquad (2)$$

Here e denotes the condensation efficiency and $\rho(x)$ is the number of droplet images per unit length of track between x and x+dx, where x is the distance from the center of the track. Let m_1 be the magnification from chamber to film and m_2 the magnification from film to slit. Then the magnification from chamber to slit is $m = m_1 m_2$ and the distribution of droplet images on the slit can be written:

$$\rho(u)du = \frac{ne}{m\sqrt{2\pi}} \exp\left(-\frac{u^2}{2}\right) du$$

$$u = x/\sigma \quad , \quad \sigma = \sqrt{2D\tau} \qquad (3)$$

where x and σ are measured in mm in the chamber. Let S be the width of the slit used, measured in mm on the slit. Then if the track is centered on the slit, the number of droplet images per unit length of track between +S/2 and -S/2 is:

$$\rho(S) = \frac{n}{m}\frac{e}{\sqrt{2\pi}} \int_{-\frac{S}{2\sigma m}}^{+\frac{S}{2\sigma m}} e^{-u^2/2} du$$

$$\rho(S) = \frac{ne}{m} \operatorname{Erf}\left(\frac{S}{2\sqrt{2}\,\sigma m}\right) \qquad (4)$$

where Erf denotes the well-known error function.[12] In the emulsions used in cloud chamber work, the diameter of a single droplet image is between 2×10^{-3} and 3×10^{-3} cm, and is considerably larger than the purely optical image in the plane of focus.[13] The size of the photographic image is therefore determined entirely by the properties of the emulsion. Individual droplet images can, however, be resolved (and consequently counted) only for lightly ionizing tracks, and provided the proper chamber operating conditions exist.[11] For heavily ionizing particles (greater than about 2 times minimum), and with chambers for which the resolution is not sufficient for droplet counting even at low ionization, the track image is essentially the result of superposition of single droplet images.

Let c denote the area of a single droplet image (in mm^2 on the slit) and let a = SL (in mm^2) be the area of the slit, where L is the length of the slit in mm. Then the probability of having i images overlap can be approximated by the Poisson distribution[14]:

$$P(i) = \frac{\lambda^i e^{-\lambda}}{i!} \tag{5}$$

$$\text{and} \qquad \lambda = \frac{\rho(S)Lc}{a} = \frac{nce}{mS} \operatorname{Erf}\left(\frac{S}{2\sqrt{2}\, m}\right)$$

Here n is the number of ions per mm of track in the chamber. The quantity λ is a measure of the average number of overlapping images.

Now, if a single drop image transmits a fraction t of the incident light, i superimposed images will transmit a fraction $t^{i^{-\gamma}}$, provided the linear part of the H-D curve is involved.[15] γ is the so-called "gamma" of the emulsion. The total transmission, relative to the background, of the film area projected through the slit

can then be written:

$$T = e^{-\lambda}\left[1 + t \sum_{i=1} \frac{\lambda^i i^{-\gamma}}{i!}\right] \qquad (6)$$

Thus a relation between transmission and the specific ionization, i.e. the number of ions per unit length of track relative to the minimum value, has been established under the various assumptions stated above. It is now of interest to investigate the behavior of T, substituting approximate numerical values for the various physical parameters:

$$D = 0.072 \text{ cm}^2\text{sec}^{-1} \quad (16)$$

$$\tau = 0.016 \text{ sec.}$$

$$m = 2.58$$

$$S = 1.5 \text{ mm.}$$

$$c = 0.19 \text{ mm}^2 \quad (13)$$

$$n_{min} = 3.9 \text{ ion pairs/mm} \quad (17)$$

$$e \sim 0.90$$

which gives for the parameters σm and λ :

$$\sigma m = 0.72 \text{ mm}$$

$$\lambda = 0.362 \text{ I}$$

where I is the specific ionization.

The properties of the film have been determined,* and the H-D curve is shown in Fig. 6. The value of γ is 1.26, and the densities (d = -log T) of tracks relative to the background fall on the

---

*This work was carried out by Mr. A. Strassenburg in connection with the design of a light source for the 48" cloud chamber.

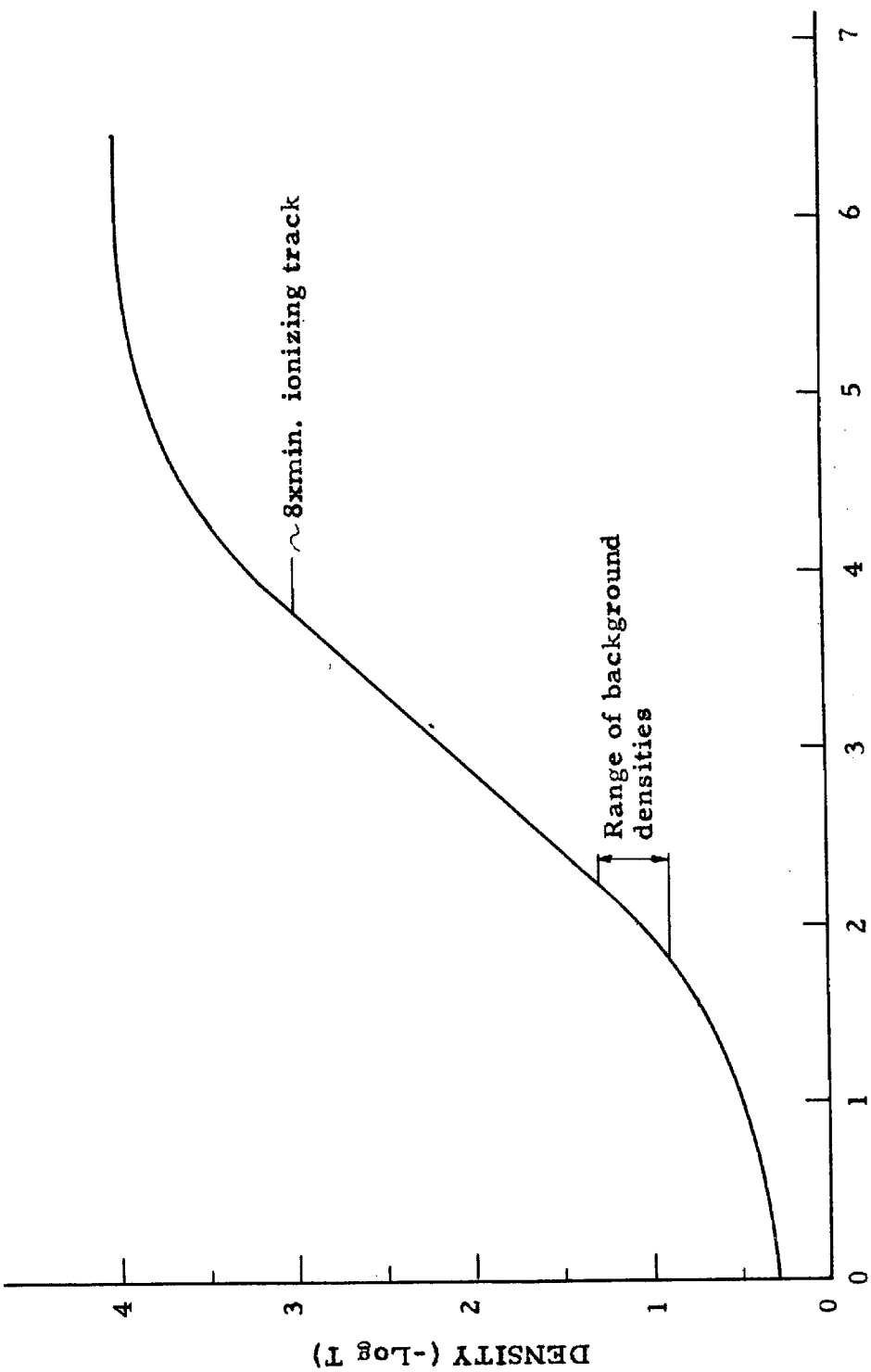

Figure 6. H-D curve for the photographic emulsion. The units of exposure are arbitrary.

linear part of the curve.

Substituting these values, the expression for the transmission becomes

$$T = e^{-0.36I}\left[1 + 0.36t\ \ (I+0.074I^2 + 0.0055I^3 + \ldots.)\right] \qquad (7)$$

The first term on the right-hand side of this expression is the contribution to the total transmission from the part of the slit not covered by droplets. The second term is the contribution from single images, the third term from double images, etc. Thus only for heavily ionizing tracks need the contributions from overlapping images be taken into account.

It is difficult to obtain an experimental value for t ; however it is unlikely that it exceeds 0.10. In Fig. 7, T is plotted as a function of I for three values of t : 0, 0.10 and 0.25. In deriving Eqn. (7) the condensation efficiency was taken as 0.90. This value is believed to be correct for ideal operating conditions; however, such conditions do not always exist, and the value of e may vary considerably for different expansions of the chamber. The effect such a variation has on the curve in Fig. 7 is to change the scale of the abscissa (Ionization) by a factor e/0.90. For instance a 10 per cent decrease in the condensation efficiency would increase the transmission for a 5x min. ionizing track by about 17 per cent, and for a 2x min track by about 11 per cent, irrespective of the value of t.

Furthermore, the background condensation also varies considerably for different expansions and throughout the chamber for each expansion. But since the range of background transmissions found experimentally, as shown in Fig. 6, is on the linear part of

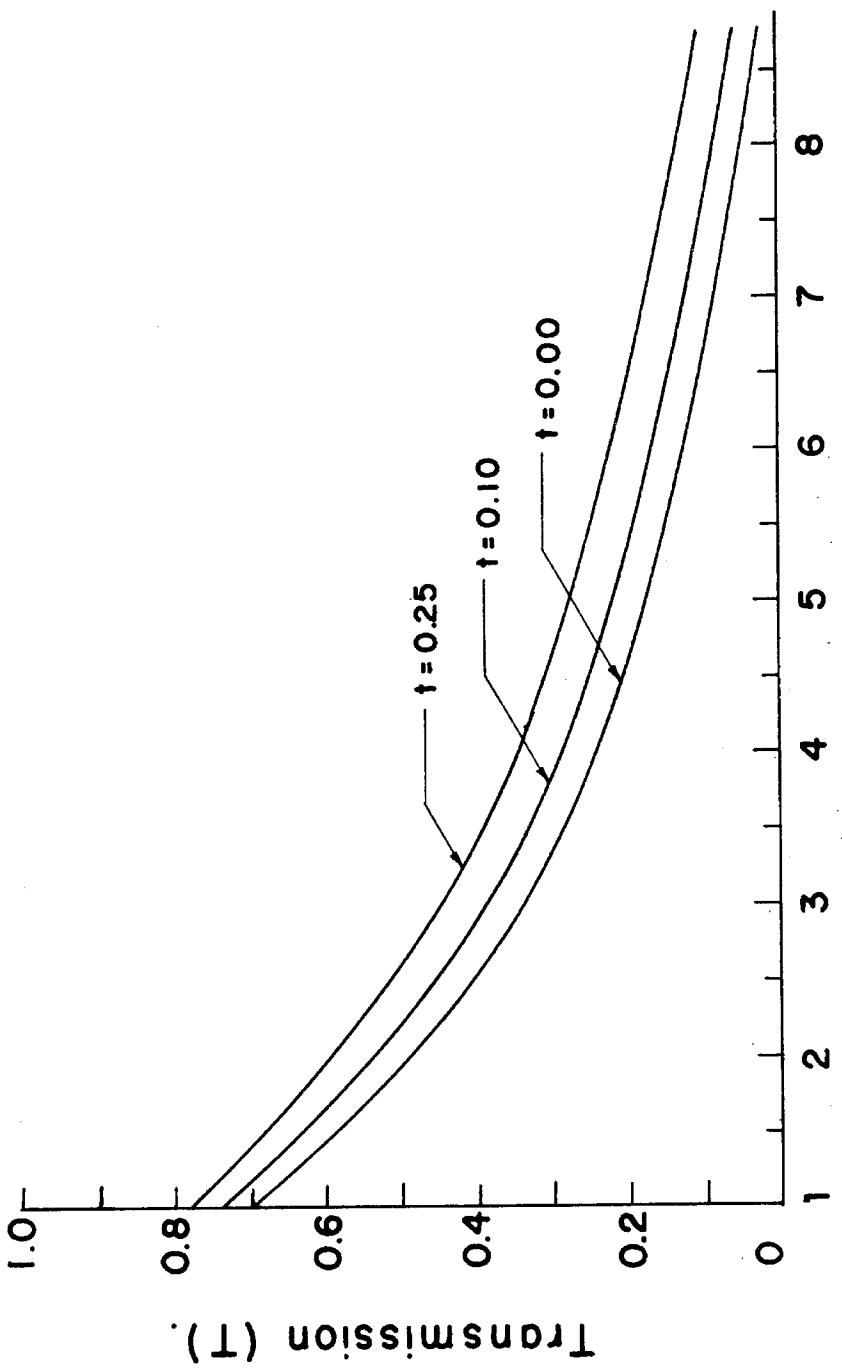

Figure 7. Theoretical curves of transmission versus ionization, computed from Eqn. (7). t is the transmission of a single droplet image.

the H-D curve, this variation will not affect the measurement of transmission. Changes in illumination of the chamber, however, will influence the measurements by changing the value of t. But it is unlikely that for any change in the illumination t will fall outside the range 0.05 to 0.25.

The transmission of an out-of-focus track can be seen to vary with the degree of out-of-focus. Let this change be measured by the ratio of areas of the images, c/c_o, when c_o is the area of the image when the track is in focus. Provided the total amount of light received is the same for both images, the transmission, t, of the image c will become:

$$t = 1 - \frac{c}{c_o}\left[1 - t_o\left(\frac{c}{c_o}\right)^{\gamma}\right] \qquad (8)$$

where t_o is the transmission of the image of area c_o. For the most likely values of t_o, i.e. in the range 0.5-.25, an increase in transmission (t) will occur for c/c_o greater than about 3, and for smaller values of c/c_o the transmission will decrease. But the changes will not affect the total transmission of the track to any appreciable extent. However the value of λ, i.e. the average number of overlapping images, is changed by a factor c/c_o, which corresponds to a change of scale of the abscissa in Fig. 7 by the same factor. For instance, for a 5x min. ionizing track the total transmission would decrease by about 60 per cent if the area of each image is doubled. For less heavily ionizing tracks the change would be correspondingly smaller.

From these considerations it is evident that the transmission of a track cannot by itself be used to determine the value of the ionization. However, if the transmission of the track is compared with the transmission of a track for which the ionization is known, it should be possible to obtain a measure which is largely independent of the various changes discussed above. This approach has been adopted to obtain an ionization-dependent parameter. The method will be described in Section 5.

4. Preliminary Measurements

The effects of various physical parameters have been investigated from a theoretical point of view, and it is now of interest to compare these results with the experimentally determined behavior of the transmission for different tracks. The parameter

$$f = 1 - T, \tag{9}$$

where T is the transmission of the track relative to a transmission value of unity for the background, was used rather than T itself, in order to have a parameter which increases with increasing ionization. The track to be measured was scanned as described in Section 2, and the out-put of the photo-tube traced on the recorder. The slit was made to scan about four to five track widths on each side of the track, in order to estimate the background density. Each track was scanned four to ten times depending upon the length of track inside the illuminated region of the cloud chamber. Reproductions of actual tracings are shown in Fig. 8. The value of f was

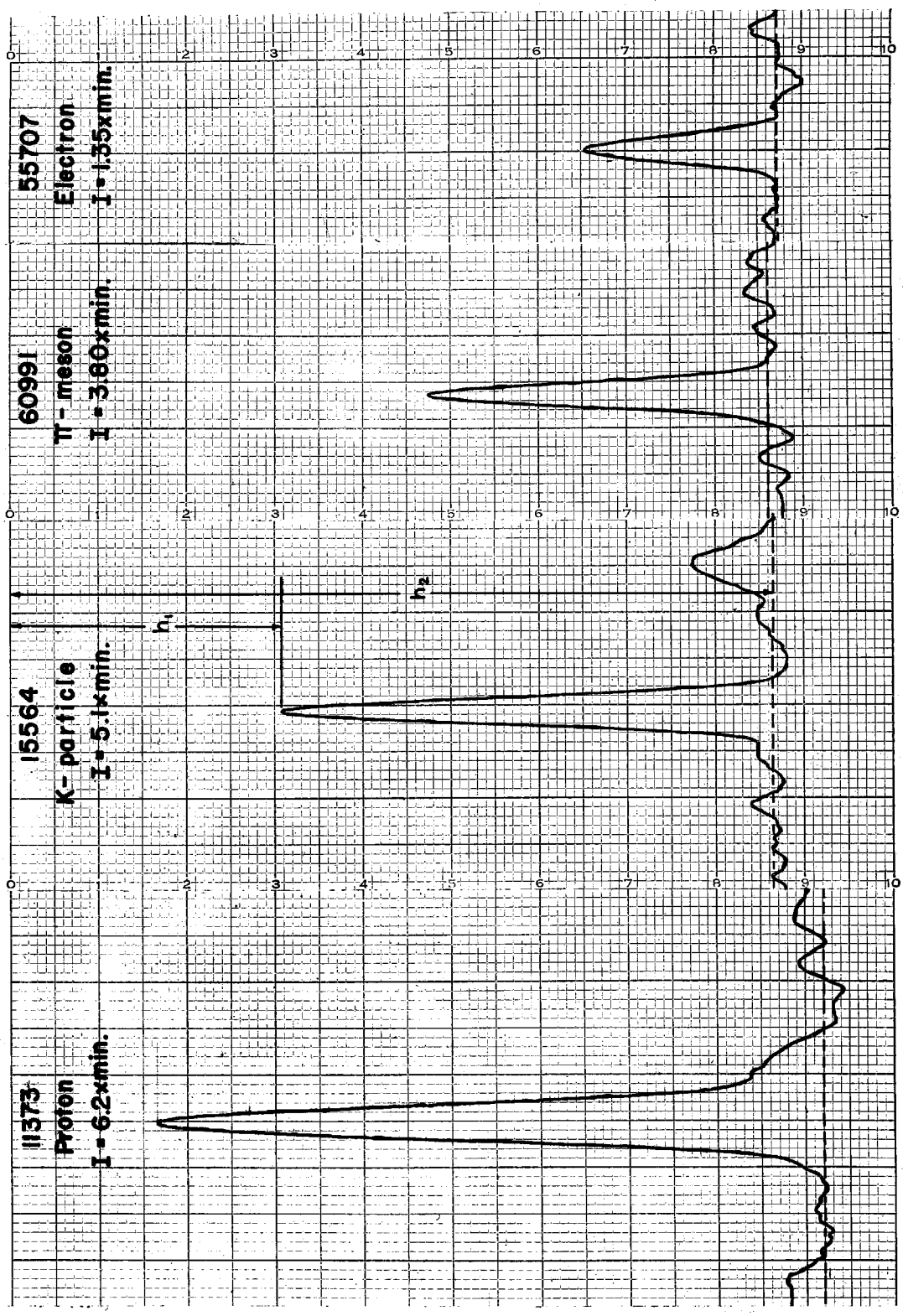

Microphotometer - tracings of various cloudchamber tracks.

Figure 8

calculated from the tracings by Eqn. (9), or as is shown in Fig. 8:

$$f = 1 - h_1/h_2 \tag{10}$$

A typical tracing with four to ten independent measurements of f along the track showed the variation in f to be about 5-15 per cent. This variation was also obtained for tracks traversing the chamber in a plane perpendicular to the line of sight, i.e. for tracks with nearly constant illumination. Thus any effect of changes in illumination could not be detected, which is in accord with the results derived theoretically. Furthermore, the background transmission varied considerably along the tracks, but no correlation between these changes and the variation in f was found; again in accord with the theoretical results. No quantitative measurements on the change in f due to out-of-focus images were made. However, for tracks with parts of the track out-of focus an increase in f was observed.

Measurements on the variation of f as a function of slit-width were made for slit-widths 0.5, 1.0, 1.5 and 2.0 mm, and the results are shown in Table II. The measured areas under the transmission curves are also shown. The results for f as a function of S can be described by the equation

$$f_S = f_{1.5} - 0.05\,(S-1.5) \tag{11}$$

where f_S is the value of f for the slit-width S, and $f_{1.5}$ is the value for S = 1.5. This behavior is exactly that to be expected from the theoretical considerations. Values of f as a function of slit-width can be computed from the curves in Fig. 7. The abscissa is changed

	S = 0.5mm		S = 1.0mm		S = 1.5mm		S = 2.0mm	
Frame	f	A	f	A	f	A	f	A
7029	0.78	1.37	0.76	1.47	0.73	1.53	0.69	1.34
7029	0.31	0.45	0.28	0.49	0.26	0.45	0.23	0.48
7029	0.24	0.43	0.22	0.40	0.19	0.39	0.16	0.37
42368	0.54	1.11	0.51	1.15	0.49	1.09	0.47	1.10
42368	0.60	1.21	0.57	1.19	0.54	1.20	0.51	1.21
46613	0.55	1.15	0.53	1.12	0.51	1.08	0.49	1.16
46613	0.35	0.64	0.32	0.63	0.30	0.65	0.28	0.64
47214	0.68	1.37	0.66	1.55	0.64	1.45	0.62	1.53
47214	0.61	1.12	0.59	1.15	0.57	1.20	0.55	1.15

Table II. Measurements of f and A, where f is the height of the transmission curve for the track, above the background, and is read off directly from the trace. Zero transmission (no light to the phototube) is equal to 1.0 on this scale. A is the area under the transmission curve, measured relative to the scale of the slit. The dimension of A is mm on the slit.

by a factor r(S):

$$r(S) = \frac{1.5}{S} \left\{ \frac{\mathrm{Erf}\left(\frac{S}{2\sqrt{2}\,\sigma m}\right)}{\mathrm{Erf}\left(\frac{1.5}{2\sqrt{2}\,\sigma m}\right)} \right\} = 2.13 \; \frac{\mathrm{Erf}\left(\frac{S}{2\sqrt{2}\,\sigma m}\right)}{S} \qquad (12)$$

The values obtained for r(S) are:

$$r(0.5) = 1.15$$

$$r(1.0) = 1.09$$

$$r(2.0) = 0.89$$

Using these values of r(S) and the curves in Fig. 7, the change in f per mm. of slit-width is found to be 0.05, independent of the value of f and the parameter t.

The areas under the transmission curves, as shown in Table II, seem to be independent of the slit width used. These measurements, however, cannot be considered significant, as is obvious from an inspection of the traces shown in Fig. 8. The uncertainties in the determination of the background transmission introduce considerable variation in the areas under the curves. These uncertainties do not affect the measurement of f to the same extent.

It is interesting to note that the values of f obtained for shower particles measured as described above, were in the range 0.20 to 0.30. This is in excellent agreement with the values obtained from Fig. 7 for tracks at minimum ionization. However, the measured values of f for heavily ionizing tracks were not in such good agreement with the values derived from the theoretical curve using visual ionization estimates.

5. The Use of Comparison Tracks

The method used for the measurements of the parameter f has been described in the previous Section, and the need for a comparison track of known ionization on the same photograph has been demonstrated in Section 3. On the majority of the photographs of interest such comparison tracks were found. These tracks were in most cases due to electrons, but penetrating shower-particle tracks were also used as comparison tracks. Occasionally π- and μ-meson tracks and also proton tracks were used when positive identification of these particles could be made. The ionization values of the comparison tracks were calculated using the measured momenta.[11] In the case of electrons the ionization values were inferred from a theoretically calculated curve shown in Fig. 9 giving ionization as a function of electron momentum. *

The same procedure of measurement of the parameter f was used for both tracks. The averages of the various values of f obtained for different scannings were computed, and the ratio (D_u) of the two average values thus obtained was calculated:

$$D_u = \frac{f(\text{unknown track})}{f(\text{comparison track})} \qquad (13)$$

In order to establish an experimental calibration curve it is necessary that the ratio D_u for the various tracks be taken relative to comparison tracks of the same ionization. This is of course not always possible, and therefore a correction must be applied to D_u.

---

*This curve is based on calculations by Dr. R. F. Christy.

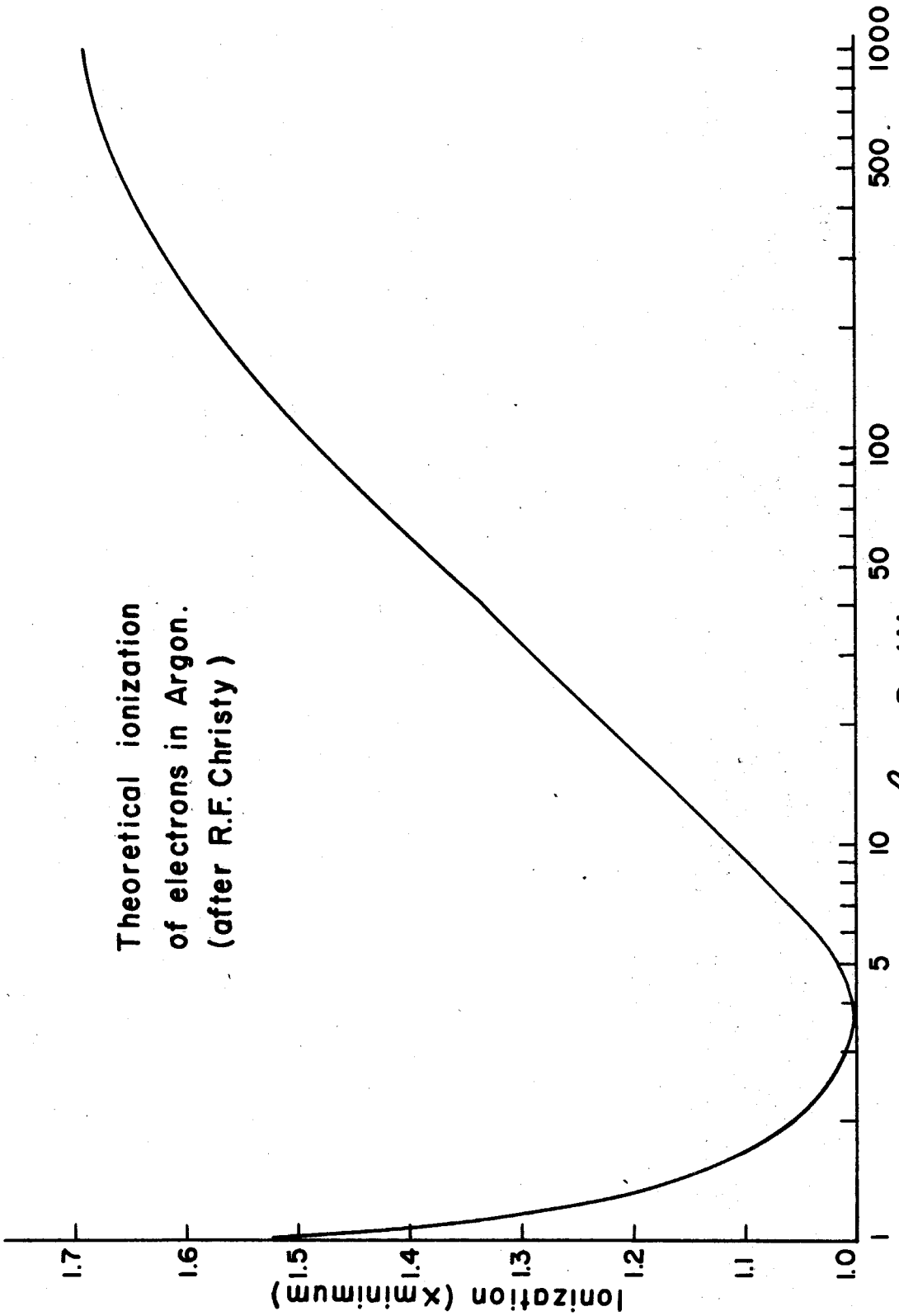

Figure 9. Theoretical ionization of electrons in argon as a function of momentum. (P in Mev/c). The mass M is measured in Mev.

Let D_c be the ratio

$$D_c = \frac{f(\text{comparison track})}{f(\text{min. ionizing track})} \tag{14}$$

Then the quantity

$$D = D_c D_u \tag{15}$$

satisfies the above requirement, where a minimum ionization track is chosen as the standard comparison track. The appropriate values of D_c for comparison tracks other than a minimum ionization track were determined from a preliminary calibration curve, giving D as a function of ionization, which was constructed using penetrating shower particles for comparison tracks. The calibration procedure will be described in Section 7. However, before attempting to correlate ionization with the parameter D, it is necessary to consider several factors depending upon the geometry of the tracks and which influence the measurements.

6. Correction Procedure

Since the photoelectric method in effect measures the transmission of the projected track images, a relation between the intensity of the light scattered by the droplets forming the track and the light received at the film must be established. Such a relation can easily be found under the assumptions that (1) the illumination is constant throughout the illuminated region of the chamber and (2) that the intensity of the light scattered in the direction of the camera lens is independent of the size of scattering droplets and the angle of scattering.

Let L and L' be proportional to the light scattered from unit area in the chamber and to the light received at the film, respectively. It can then be shown that[11]

$$L' = \frac{\pi a^2}{4} \cdot \frac{L}{\ell^2} \cdot \left(\frac{B}{B'}\right) \cos\phi \tag{15}$$

where a is the diameter of the camera stop, B and B' denote the areas of the scattering droplets in the chamber and on the film respectively, ℓ is the distance between the scatterer and the camera lens, and ϕ is the angle of inclination of the scattering surface relative to the line of sight. Using the relations:

$$\begin{aligned} \ell &= F\left(1 + \frac{1}{m_1}\right) \\ m_1 &= (B'/B)^{1/2} \\ N &= a/F \end{aligned} \tag{16}$$

where F is the focal length of the camera lens, m_1 is the magnification, and N is the numerical aperture, the above equation can be written:

$$(L'/L) = \pi/4 \left[\frac{N}{1+m_1}\right]^2 \cos\phi \tag{17}$$

The fractional change in intensity $\left(\frac{\partial L'}{L'}\right)$ due to a change in magnification can be shown to amount to only a few percent:

$$\left(\frac{\partial L'}{L'}\right) = \frac{2m_1}{m_1+1} \frac{\partial \ell}{\ell} \simeq 2 \text{ per cent} \tag{18}$$

where $m_1 = 1/6.3$ and $(\partial \ell/\ell)_{max} \simeq$ 7-8 percent. Thus the only correction that need be taken into account is the correction for the dip of the track relative to the line of sight. The angle ϕ can be found

from the stereoscopic projection of the photographs in the same manner as for momentum measurements.[2] The validity of the assumptions stated above cannot easily be ascertained. The illuminated region does not appear, upon a visual examination, to be of uniform intensity; however, since the electron tracks to which the unknown tracks are compared are chosen so as to be in the same part of the chamber, the non-uniformity of the illumination does not have to be taken into account. Measurements on the scattered intensity as a function of scattering angle in a cloud-chamber have been reported.[18] From these data it appears that the variation in relative intensity at a scattering angle of 90 degrees is less than 1 per cent per degree. The accuracy of the present measurements does not warrant a correction for this effect.

7. Calibration

In order to establish an empirical relation between the measured parameter D and ionization, twelve π-μ decays, for which both momenta could be measured were selected. These events yielded sixteen tracks which could be measured photometrically. The Q-values were calculated to check the identification, and in all cases was the computed energy release consistent, within the errors of measurement, with the currently accepted value for π-μ decay.

The values of the expected ionizations were calculated from the measured momenta and corrected for the dip of the tracks in the chamber. And in each case was the parameter D_u computed from the micro-photometer tracings in the manner described in

Section 5. The values of D_u for the six cases with minimum ionizing comparison tracks (i.e. $D_c = 1$) were plotted against the theoretical ionization, and a straight line could be fitted to the experimental points with very little scatter. The ionization values for these cases were in the range 2 to 4.x minimum. In the other cases, the values of D_c for the electron comparison tracks, corresponding to the theoretical ionization values obtained from Fig. 9, were then inferred from this preliminary curve, and the measured parameters D_u were corrected for the ionization of the comparison track according to Eqn. (15). No correction was applied for the dip of the electron tracks; only tracks with little or no dip were used. The final calibration curve obtained in this manner is shown in Fig. 10. The errors assigned to each case were computed from the momentum errors.

As a check on the internal consistency of the calibration procedure Table III has been prepared. The mass values (column 5) have been computed for each π-μ decay from the measured momenta (column 1) and the ionization found by using the calibration curve (column 4). The correction factors for dip are given in column 3. The errors quoted in the mass values were computed from the momentum errors only. It is seen that the calculated masses are consistent with the accepted values. The mean values are found to be $M_\pi = 276 \pm 12 m_e$ and $M_\mu = 208 \pm 7 m_e$.

The procedure for calculating the ionization of an unknown track from the tracings can be summarized as follows: (1) the values of f are calculated in the manner shown in Fig. 8 ($f = 1 - h_1 h_2$), for both the unknown track and the comparison track, (2) the ionization

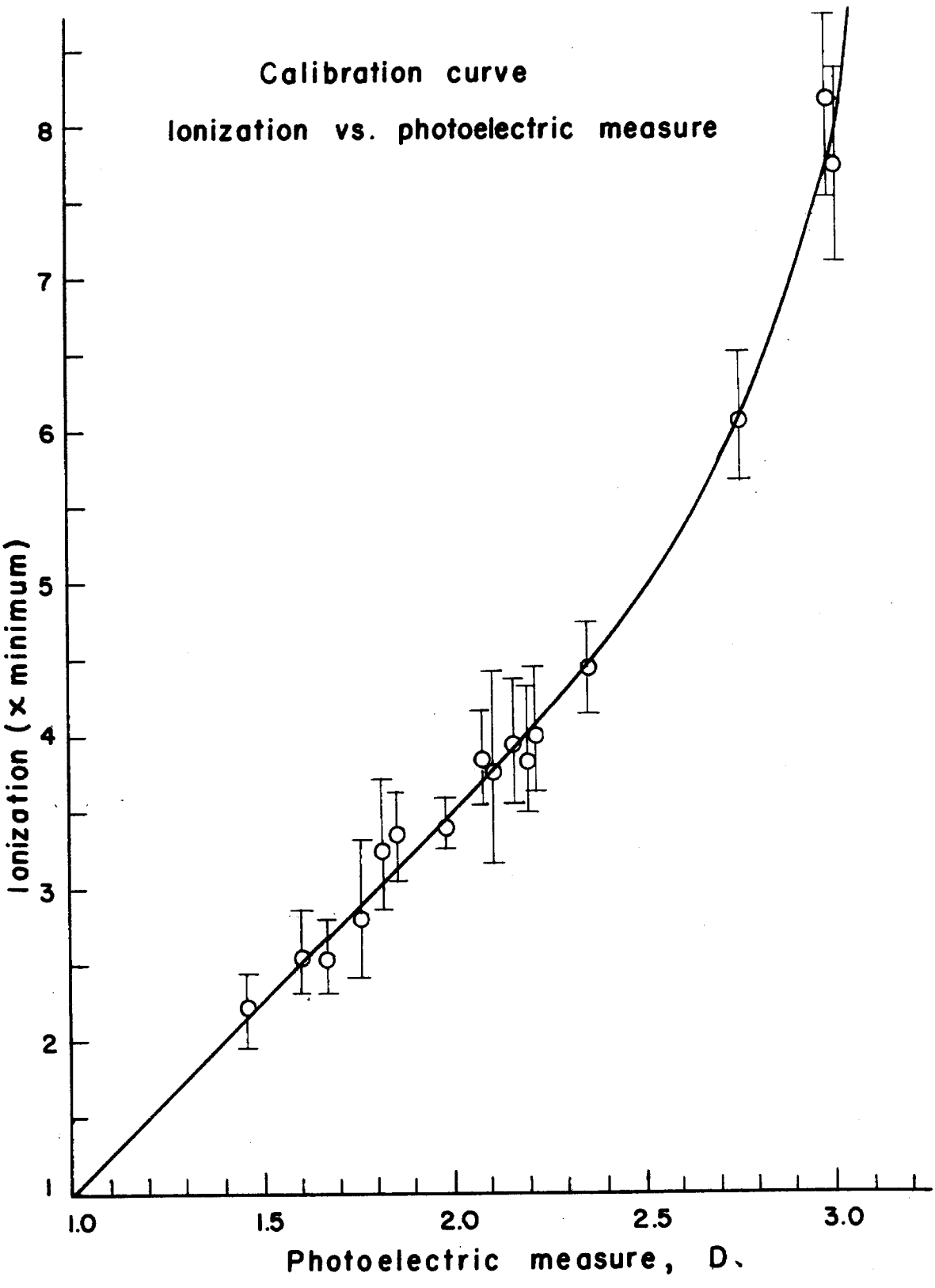

Figure 10. Calibration curve; photoelectric measure D, vs. ionization. The experimental points represent π- and μ-meson for which the ionizations were obtained from the measured momenta. The uncertainties in ionization result from the errors of measurement of the momenta.

Frame No.	(1) P(Mev/c)	(2) D	(3) cosφ	(4) I	(5) M (m_e)
16202	62 ± 2	1.98	.85	2.88	206 ± 20
36017	86 ± 12	1.76	1.00	2.86	286 ± 40
36017	52 ± 8	2.11	.97	3.63	205 ± 30
45225	75 ± 4	1.82	.99	3.00	258 ± 20
45225	37 ± 3	3.02	.79	6.15	211 ± 10
48555	53 ± 3	2.76	.91	5.50	275 ± 20
48555	60 ± 6	2.22	.76	3.08	210 ± 20
49655	78 ± 10	1.81	.93	3.69	312 ± 40
49655	70 ± 7	1.60	.98	2.40	204 ± 20
53012	108 ± 7	1.45	.99	2.08	274 ± 30
53012	47 ± 4	2.14	.99	3.82	193 ± 15
59268	61 ± 3	2.36	1.00	4.46	278 ± 15
59268	78 ± 4	1.68	.95	2.52	230 ± 20
60967	42 ± 2	3.00	1.00	8.0	273 ± 15
60967	50 ± 4	2.20	1.00	4.00	212 ± 20
64831	51 ± 2	2.12	.97	3.68	204 ± 15

Table III. Ionization measurements on π-μ decays used in constructing the calibration curve. The table has been prepared to show the internal consistency of the calibration procedure. The measured parameter D (column 2) was used to find the "apparent" ionization by the use of the calibration curve (Fig. 7). The dip correction (column 3) was then applied, and the final ionization values (column 4) together with the measured momenta (column 1) yielded the mass values (column 5). The errors quoted for the masses were computed from the momentum errors only.

A plot of momentum versus ionization for these cases is shown in the accompanying figure.

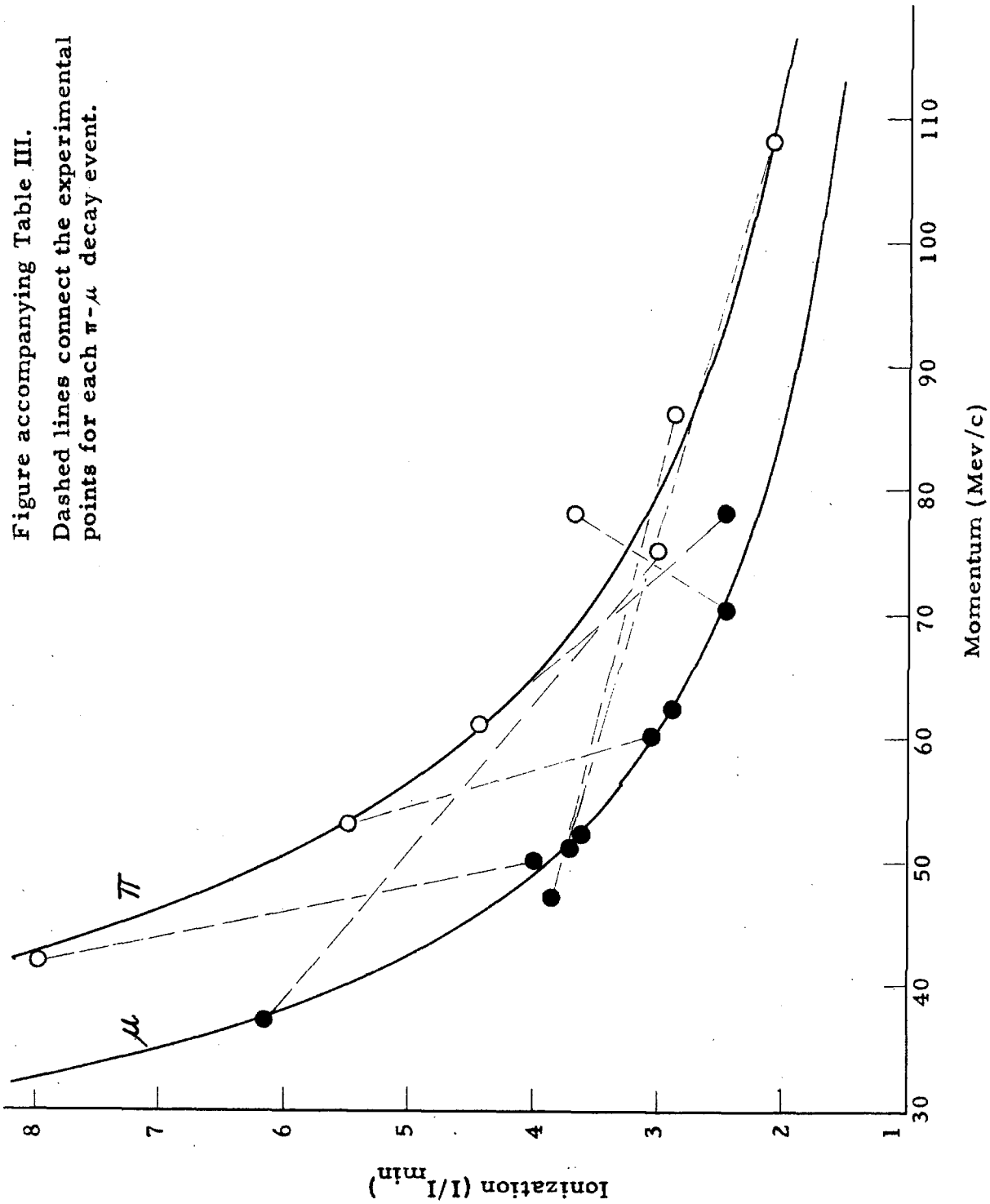

Figure accompanying Table III.
Dashed lines connect the experimental points for each π-μ decay event.

of the comparison track, if an electron, is found using Fig. 9, and the value of D_c corresponding to this ionization is read from the calibration curve, (3) the ratio $D_u = f_u/f_c$ is then multiplied by D_c to give D, (4) from which the apparent ionization (I') is found using the calibration curve; (5) the final ionization (I) is then found after correction for dip ($I = I'\cos\phi$).

8. Errors of Measurement

Examination of sets of tracings allow an estimation of the accuracy of the method to be made, exclusive of any systematic errors. A typical tracing with four to ten independent measurements of f shows the variation in f to be about 5-15 per cent. This is of the right order of magnitude to be accounted for by the Landau fluctuations.[18] Butterworth[8] estimates that, for a 2-3x minimum ionization track, the fluctuation is about $20/\sqrt{\ell}$ per cent, where ℓ is the track length in cm.

Although care is taken to use a comparison track in the same part of the chamber as the unknown track, variations in illumination and the degree of out-of-focus of the images probably introduce considerable uncertainties in the measured ionization, and the uncertainties due to errors of measurement of the angle of dip of the track may also be large, especially for large angles. But on the basis of Table III it seems reasonable to conclude that the errors in the ionization values do not exceed 10-15 per cent. Fortunately, a considerably larger error can be tolerated in the ionization than in the momentum (for ionization greater than twice minimum) to obtain a mass measurement of given accuracy.[2]

9. Application of Method

The method was used to measure the ionization of 50 cloud chamber tracks, and the results are given in Table IV. A few measurements on charged V-particles found in the 48" cloud chamber have also been performed, and these are included in the table. The measured parameters D and the dip corrections are given, together with the final values of the ionization, and the masses computed from these values and the measured momenta. The errors quoted for the ionization values are probable errors of measurement, and the errors assigned to the final masses were computed from the combined probable errors of ionization and momentum. A histogram of measured masses is shown in Fig. 11. The peak which occurs at about 1840 m_e includes only positive secondaries of neutral V-particles, with one exception; this being a positive secondary of a charged V-particle. It is seen that these cases are consistent with protons. The peak at about 1050 m_e are all charged V-primaries except for three positive secondaries of neutral V-particles. This peak presumably contains K-particles. The light meson peak at about 280 m_e is consistent with a π-meson. Apparently, no μ-mesons were included in the sample measured.

A reproduction of a frame with tracks particularly suited for ionization measurements is shown in Fig. 12. The measurements performed on the tracks labeled as shown in the figure are given in detail in Table V. Track A is most likely due to a π-meson. The errors of measurements appear to exclude the possibility of the track being due to a μ-meson. Track B, on the other hand, is

Frame No.	(1) P (Mev/c)	(2) D	(3) cos ϕ	(4) I/I_{min}	(5) $M(m_e)$	(6) Type of event*
7029	185± 20	3.00	0.95	7.4±0.6	1140±150	V^-, prim.
11373	450±100	2.28	0.92	3.90±0.4	1870±400	V^o, pos.sec.
14345	425± 50	1.71	0.89	2.40±0.3	1200±200	-"-
14539	390±100	2.34	0.55	2.22±0.4	1050±250	-"-
15564	350± 50	1.83	0.95	2.90±0.4	1170±200	n.d.p. (pos.)
16798	230± 30	2.48	1.00	4.83±0.6	1100±200	V^o, pos.sec.
-"-	112± 10	1.76	1.00	2.37±0.3	310± 50	V^o, neg.sec.
17671	415± 50	2.22	1.00	4.06±0.3	1780±150	n.d.p. (pos.)
24964	270± 50	2.32	0.93	4.00±0.5	1140±200	n.d.p. (neg.)
25026	245± 30	2.35	1.00	4.40±0.3	1100±150	-"-
25343	185± 60	2.23	0.94	3.90±0.5	770±320	V^+, prim.
26361	475± 50	3.36	1.00	3.36±0.4	1780±200	V^o, pos.sec.
30047	575±100	1.77	1.00	2.85±0.4	1900±500	-"-
-"-	440± 80	2.35	1.00	4.45±0.6	2000±400	-"-
30335	128± 9	2.96	1.00	7.50±1.0	800±200	n.d.p. (neg.)
-"-	56± 4	2.57	0.98	5.05±0.4	275± 30	n.d.p. (pos.)
30514	475± 50	2.22	0.94	3.80±0.4	1950±200	V^o, pos.sec.
32530	465±100	1.26	0.99	1.63±0.2	930±210	V^-, prim.
36091	410± 40	2.37	1.00	4.50±0.5	1880±200	V^o, pos.sec.
37264	310± 50	1.99	1.00	3.45±0.4	1170±200	-"-
-"-	125± 20	2.14	0.50	1.92±0.2	290± 40	V^o, neg.sec.
37873	410± 80	2.23	1.00	4.08±0.6	1750±300	V^o, pos.sec.
38688	286± 30	1.72	0.92	2.55±0.3	860±120	V^+, prim.
41646	320± 40	2.92	0.96	6.82±0.7	1890±250	V^+, sec.
42368	245± 15	2.31	1.00	4.30±0.2	1080±100	V^-, prim.

	(1)	(2)	(3)	(4)	(5)	(6)
43955	109± 10	1.62	0.96	2.35±0.4	305± 50	V^+, sec.
46613	368± 30	1.66	0.86	2.25±0.3	990±110	V^+, prim.
46906	280± 50	2.90	0.94	6.60±0.8	1620±300	V^o, pos. sec.
47214	172± 15	3.00	0.96	7.50±0.8	1070±120	V^+, prim.
49169	215±100	2.08	0.87	3.05±0.2	750±350	-"-
49317	415± 50	2.14	1.00	3.80±0.4	1700±200	V^o, pos. sec.
53495	600±100	1.83	1.00	3.04±0.4	2050±400	-"-
55707	230± 15	2.52	0.94	4.65±0.3	1080±100	V^+, prim.
56646	360± 50	2.50	0.96	4.70±0.5	1700±250	V^o, pos. sec.
59180	560± 75	1.71	1.00	2.72±0.3	1800±300	-"-
-"-	70± 10	2.96	0.50	3.70±0.3	280± 40	V^o, neg. sec.
60452	255± 60	2.84	0.54	3.60±0.4	990±250	V^+, prim.
60991	70± 10	2.20	1.00	4.00±0.5	295± 50	V^+, sec.
62442	380± 50	2.48	1.00	4.85±0.3	1830±200	V^o, pos. sec.
63526	470± 75	2.33	0.97	4.22±0.3	2050±250	-"-
63804	475± 50	1.96	1.00	3.35±0.4	1800±200	-"-
71837	480± 50	2.12	0.97	3.68±0.4	1920±200	-"-
6823[a]	225± 17	2.32	0.93	4.10±0.3	965±100	V^+, prim.
11365[a]	137± 11	1.42	0.93	1.86±0.2	310± 50	V^-, sec.
18571[a]	385±100	1.76	0.96	2.71±0.3	1225±200	V^+, prim.
-"- [a]	156± 10	1.33	0.84	1.50±0.2	290± 50	V^+, sec.
20445[a]	230± 11	2.25	0.93	3.78±0.4	940±100	V^+, prim.

	(1)	(2)	(3)	(4)	(5)	(6)
20445[a]	210± 20	1.10	1.00	1.27±0.2	300± 50	V^+, sec.
29312[a]	164± 15	2.83	0.94	6.10±0.5	905±100	V^+, prim.
30166[a]	202± 11	2.29	0.97	4.12±0.4	870±150	V^+, prim.

Table IV. Data on 50 cases for which ionization measurements were made. The measured parameter D (column 2) was used to find the "apparent" ionization by the use of the established calibration curve (Fig. 8). The dip correction (column 3) was then applied; and the final ionization values (column 4) together with the measured momenta (column 1) yielded the mass values (column 5). The type of event is described in column 6.

*Abbreviation:

prim.	=	primary particle.
sec.	=	secondary particle.
pos.	=	positive.
neg.	=	negative.
n.d.p.	=	non-decaying particle.

[a] Measurements of events in the 48" chambers.

A plot of momentum versus ionization for these cases is shown in the accompanying figure.

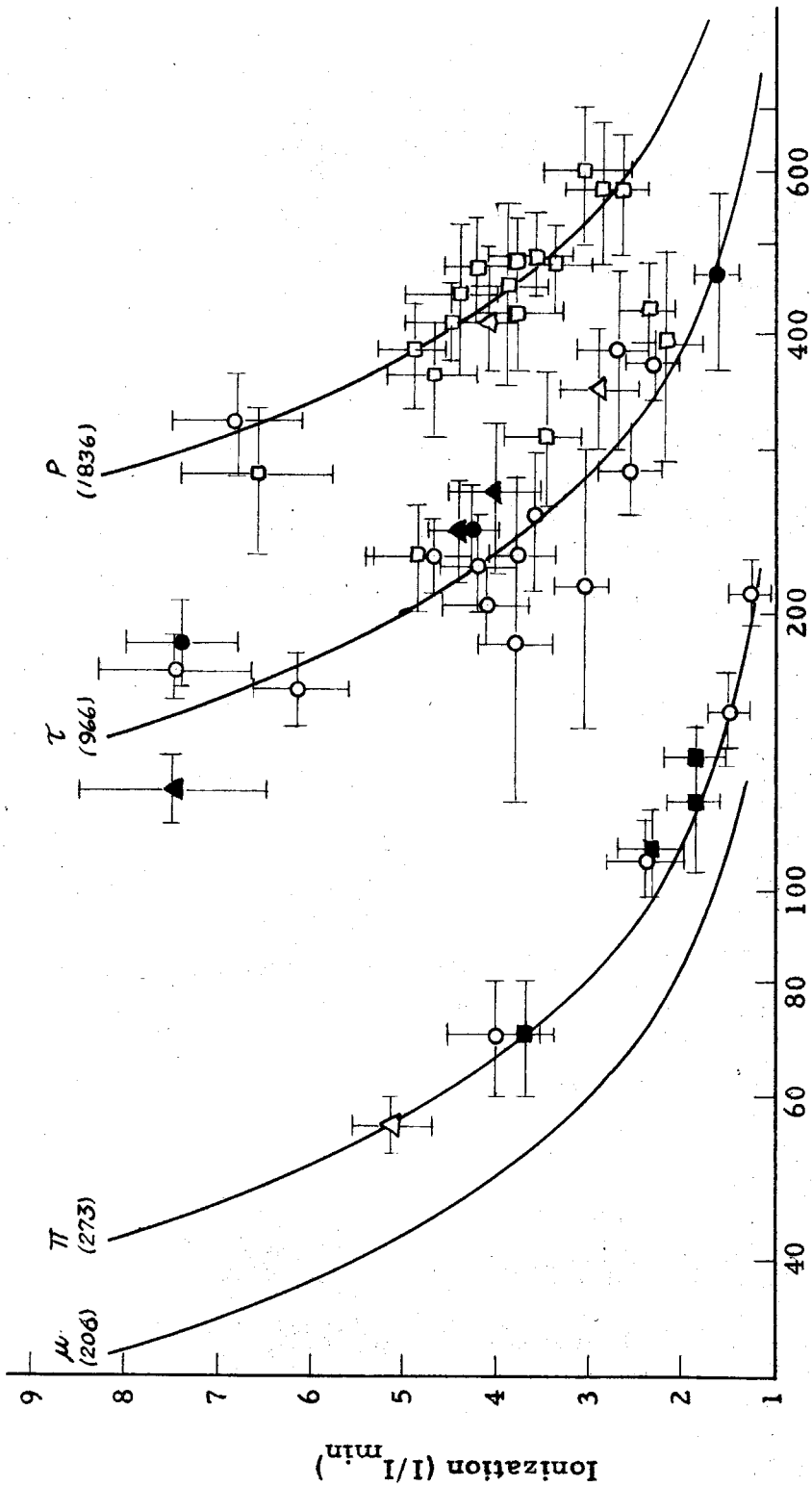

Figure accompanying Table IV. The experimental points are:
○ V^+, prim. and sec., □ V^o, pos. sec., △ pos. n.d.p.
● V^- -"- , ■ V^o, neg. sec., ▲ neg. n.d.p.

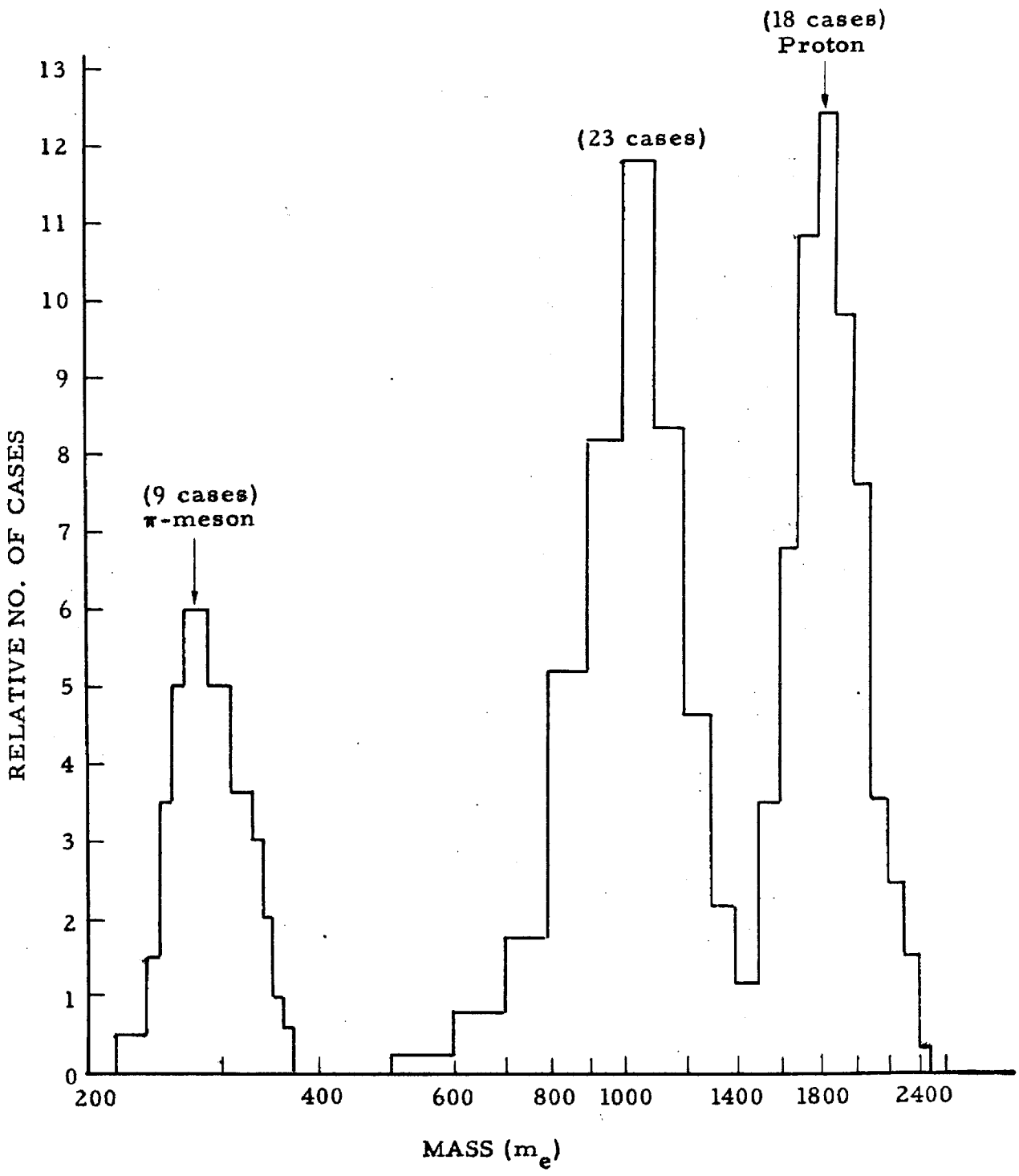

Figure 11. Histogram of the measured masses (listed in Table IV). Equal area is given to each case, and the ordinates are adjusted according to the errors of measurement. A logarithmic scale is used for the abscissa.

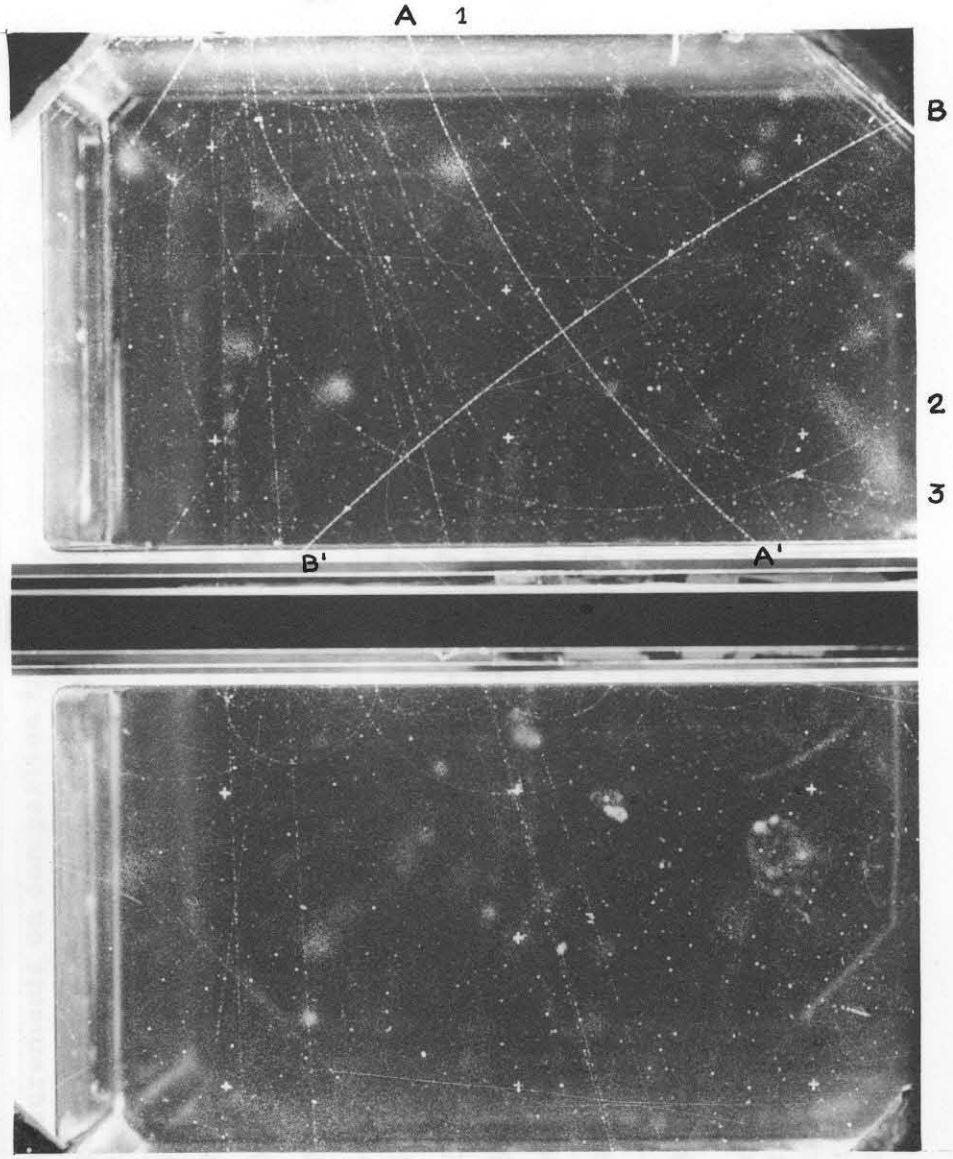

Figure 12. Event No. 30335 showing tracks particularly suited to ionization measurements. The result of the measurements on the tracks labeled A, B, 1, 2, and 3 are given in Table V.

The ionization values obtained for A and B are:

$$\text{A: } (I/I)_{min} = 5.02^{+.34}_{-.28}$$

$$\text{B: } (I/I)_{min} = 7.50^{+2.50}_{-1.15}$$

giving mass values:

$$\text{A: } M = 274^{+12}_{-10}\ m_e$$

$$\text{B: } M = 800^{+160}_{-\ 80}\ m_e$$

Comparison particle	P (Mev/c)	cos ϕ	$(I/I_{min})'$	D_c	f_c
1. (Shower particle)	-	1.00	1.00	1.00	0.30 ± 0.02
2. Electron	30 ± 5	0.98	1.36	1.15	0.35 ± 0.05
3. Electron	17 ± 4	0.97	1.26	1.11	0.32 ± 0.02

Measurements on comparison tracks

Unknown particle	f_u	Comparison track	D	$(I/I_{min})'$	cos ϕ	$(I/I_{min})'$	P (Mev/c)	M (m_e)
Track A	$0.77 \pm .03$	1	2.57	5.14	0.98	5.05	56 ± 4	275
-"-	-"-	2	2.53	5.00	-"-	4.90	-"-	272
-"-	-"-	3	2.59	5.24	-"-	5.14	-"-	280
-"-	-"-	Mean	$2.56 \pm .10$	$5.12^{+.36}_{-.30}$	-"-	$5.02^{+.34}_{-.28}$		274^{+12}_{-10}
Track B	$0.89 \pm .04$	1	2.96	7.50	1.00	7.50	128 ± 9	800
-"-	-"-	2	2.93	7.22	-"-	7.22	-"-	785
-"-	-"-	3	2.99	7.74	-"-	7.74	-"-	815
-"-	-"-	A	2.97	7.55	-"-	7.55	-"-	805
-"-	-"-	Mean	$2.96 \pm .15$	$7.50^{+2.50}_{-1.15}$	-"-	$7.50^{+2.50}_{-1.15}$		800^{+160}_{-80}

Measurements on unknown tracks

Table V. Ionization measurements on two heavily ionizing particles (Frame No. 30335), Fig. 12). f is essentially the transmission of the track relative to the background. The subscripts u and c refer to unknown track and comparison track respectively. D is computed as described in the text. ϕ is the angle of "dip" of the track. The errors quoted for the mean values are computed from the combined errors of measurements.

probably due to a K-particle. In this case the errors of measurement are rather large because of the steepness of the calibration curve in this range.

It is also of interest at this point to compare some of the measured ionization values for heavily ionizing primary particles with the visual estimates. The visual estimates were made by three independent observers and a range of possible ionization assigned.[2] The data are given in Table VI, where the errors quoted for the measured values are probable errors calculated from repeated tracings. It is seen that the values obtained by the two methods are closely correlated. In only two cases do the ranges of ionization not overlap, the measured values being somewhat higher. The mass estimates obtained for these two cases are about 800-100m_e using the measured ionization values and about 400-600 using the visual estimates. The masses calculated for the other cases using both estimates are all consistent with the masses of K-particles.

10. Limitations of Method

The method has several limitations. Primarily the necessity of requiring a comparison track in the same part of the chamber as the unknown track eliminates many cases for which a measurement of ionization would be useful. It is therefore of interest to look into the possibility of obtaining a reasonable estimate of ionization for the case where no such comparison track can be found. For this purpose the variations in the values of f_c and D_c for fifteen

Frame No.	I/I_{min}, visual	I/I_{min}, measured
7029	5.0 - 10.0	$7.4 \pm .6$
25343	1.5 - 2.0	$3.9 \pm .5$
32530	1.0 - 1.5	$1.6 \pm .2$
38688	1.5 - 2.5	$2.6 \pm .3$
42368	3.5 - 7.0	$4.3 \pm .2$
46613	1.7 - 3.5	$2.3 \pm .3$
47214	3.0 - 6.0	$7.5 \pm .8$
49169	1.7 - 3.5	$3.1 \pm .2$
55707	3.0 - 6.0	$4.7 \pm .3$
60454	4.0 - 10.0	$3.6 \pm .8$

Table VI. Comparison of measured and visually estimated ionization.

representative comparison tracks were investigated. These parameters give D in terms of the measured values of f_c by the relation:

$$D = \left(\frac{f_u}{f_c}\right) D_c = D_u D_c \qquad (15)$$

as shown in Section 5. The mean values and the standard deviations were found to be:

$$\overline{f}_c = 0.30 \pm 0.04$$

$$\overline{D}_c = 1.15 \pm 0.04$$

The value of D_c given above corresponds to an electron track with momentum P = 45 Mev/c. Although the values of f_c seem to be distributed over a fairly narrow range, the applicability of the method in the absence of a comparison track is doubtful. Using the mean values and standard deviations given above, a 3x minimum ionizing particle would have a probable error in the ionization of about twenty-five per cent. It appears that comparable accuracy can be obtained in a much more expedient manner by visual estimates.

Furthermore, the range in ionization for which the method can be employed is limited. Ionization values greater than 7-8x minimum cannot be measured. The calibration curve (Fig. 10) exhibits a saturation effect for values of D exceeding 3.0, corresponding to about 8x minimum. The accuracy of measurement in this range is furthermore very poor, due to the steepness of the slope of the calibration curve. The method must also be used with caution for lightly ionizing tracks, i.e. less than 2x minimum. Useful upper limits to the ionization can however be obtained in this range.

11. Suggested Improvements of the Method

The usefulness of photometric determination of ionization of cloud chamber tracks has been demonstrated. However, the method employed in making the measurements is of a preliminary nature, and several improvements can possibly be made.

A considerable amount of time, on the average about one hour, is required to obtain a measurement of the ionization of a particle. This time could possibly be shortened by displaying the out-put of the photo-tube on an oscilloscope screen instead of using the Speedomax recorder. A vibrating slit, or an arrangement with a rotating mirror sweeping the image of the track past the slit would accomplish this.

The use of a different parameter could be investigated in more detail, although it seems unlikely that greater accuracy would be obtained by such changes. However, for the measurements of ionization greater than 8x minimum, a different approach must be used. It is possible that estimates of ionization in this range could be obtained by using the track-width as a parameter. However, no changes in track-width (or σ m, discussed in Section 3) were detected in the range of ionization investigated.

12. List of Figures

FIG. NO.	TITLE	PAGE
1.	The microphotometer and associated electronic apparatus.	3
2.	A close-up view of the microphotometer	4
3.	The slit and the image of a heavily ionizing cloud chamber track	5
4.	Block diagram of microphotometer circuit	7
5.	Schematic diagram of the degrees of freedom of the microphotometer	8
6.	H-D curve for the photographic emulsion	16
7.	Theoretical curve of transmission vs. ionization	18
8.	Microphotometer-tracings of various cloud chamber tracks	21
9.	Theoretical ionization of electrons in argon	26
10.	Calibration curve, photoelectric measure D vs. ionization	31
11.	Histogram of the measured masses	38
12.	Event No. 30335 showing tracks particularly suited for ionization measurements	39

Figures Accompanying Tables:

Table III	A plot of momentum versus ionization for the cases given in the Table.	32A
Table IV	A plot of momentum versus ionization for the cases given in the Table.	37A

13. References

1. R. B. Leighton and S. D. Wanlass, Phys. Rev. 86, 426 (1952)
2. Leighton, Wanlass, and Anderson, Phys. Rev. 89, 148 (1953)
3. York, Leighton, and Björnerud, Phys. Rev. 90, 167 (1953)
4. York, Leighton, and Björnerud, Phys. Rev. 95, 159 (1953)
5. Hazen, Phys. Rev. 65, 259 (1944)
6. E. W. Cowan, Phys. Rev. 94, 161 (1954)
7. S. von Friesen and K. Kristiansson, Arkiv för Fysik 4, 505 (1952)
8. Report of the Bagneres Conference, 1953 (Unpublished)
9. A. W. Vance, Rev. Sci. Instr. 7, 489 (1936)
10. Elmore and Sands: Electronics, , McGraw Hill, N.Y. (1949)
11. Das Gupta and Ghosh, Rev. Mod. Phys. 18, 225 (1946)
12. Nat. Bur. Stand.: Tables of Probability Function (1941)
13. J. S. Wilson: The Principles of Cloud-Chamber Techniques. Cambridge (1951)
14. H. Cramer: Mathematical Methods of Statistics, Princeton University Press (1946)
15. C. E. K. Mees: The Theory of the Photographic Process, MacMillan, N. Y. (1942)
16. Rossi and Staub: Ionization Chambers and Counters. McGraw Hill, N. Y. (1949)
17. Sen Gupta, Proc. Nat. Inst. Sci. Ind. 9, 295 (1943)
18. Landau. J. Phys. USSR, 8, 201 (1944)

II. CLOUD CHAMBER STUDY OF CHARGED V-PARTICLES

1. Introduction

The original observation of the decay of a charged V-particle was made by Rochester and Butler in 1947.[1] Since then, extensive investigations of the nature of these decay events have been carried out by many laboratories, and a great variety of experimental evidence has been presented. The evidence has come from three distinct experimental sources, viz. cloud chambers in magnetic fields,[2-6] multi-plate cloud chambers[7] and photographic emulsions,[8-11] and has been interpreted in terms of a number of different particles.

There is now convincing evidence for the existence of at least four different types of charged V-particles: (a) τ-meson (mass $\sim$ 965 m_e) with its characteristic decay into three charged π-mesons,[10] (b) K-meson (mass $\sim$ 1000 m_e), decaying into a μ-meson and probably two or more neutral particles, (c) V_1^+-particle (positive, mass $\sim$ 2400 m_e), decaying into a proton (or a neutron) and probably a neutral (or positive) π-meson,[9-11, 12] and (d) "cascade" particle (negative, mass $\sim$ 2600 m_e), decaying into a neutral V-particle and a charged π-meson.[4, 13] Observations indicate however, that not all V-particles of mass less than nucleonic mass decaying into a light charged meson (π or μ) can be K-mesons. The existence of the χ-meson was postulated to explain these observations.[9] But the evidence for this much discussed χ-meson (mass $\sim$ 1250 m_e), decaying into a charged π-meson and one neutral particle is at present not very firm, and the possibility of

identifying this type of decay with an alternate mode of decay of the τ-meson has been considered. The similarity of the observed masses of the charged τ-meson and the neutral θ-meson decay (mass $\sim$971 m_e, and decaying into two charged π-mesons) lends support to this interpretation. The possibility of identifying the κ-meson decay with an alternate mode of decay of the τ-meson has also been discussed.[9]

It is the object of this work to present additional evidence regarding the nature of κ- and χ-meson decays and the existence of the heavy positive V-particle. The cascade decay of heavy negative particles referred to above is not discussed nor is any analysis of τ-meson decays included.

2. Apparatus and Measuring Techniques

The apparatus used in this experiment was a counter-controlled double cloud chamber operated in a magnetic field (Fig. 1) and has been described in detail by Leighton et al.[14] At the time the present work was begun the cloud chamber had already been operated for long periods of time and several of the events selected for inclusion in this study were obtained during this earlier period. Several improvements and modifications however, have been made since the work of Leighton et al. was reported. These improvements were based on the experience gained during the earlier operation period and were all made on the suggestions of Drs. Leighton and York, who also carried most of them out and shared

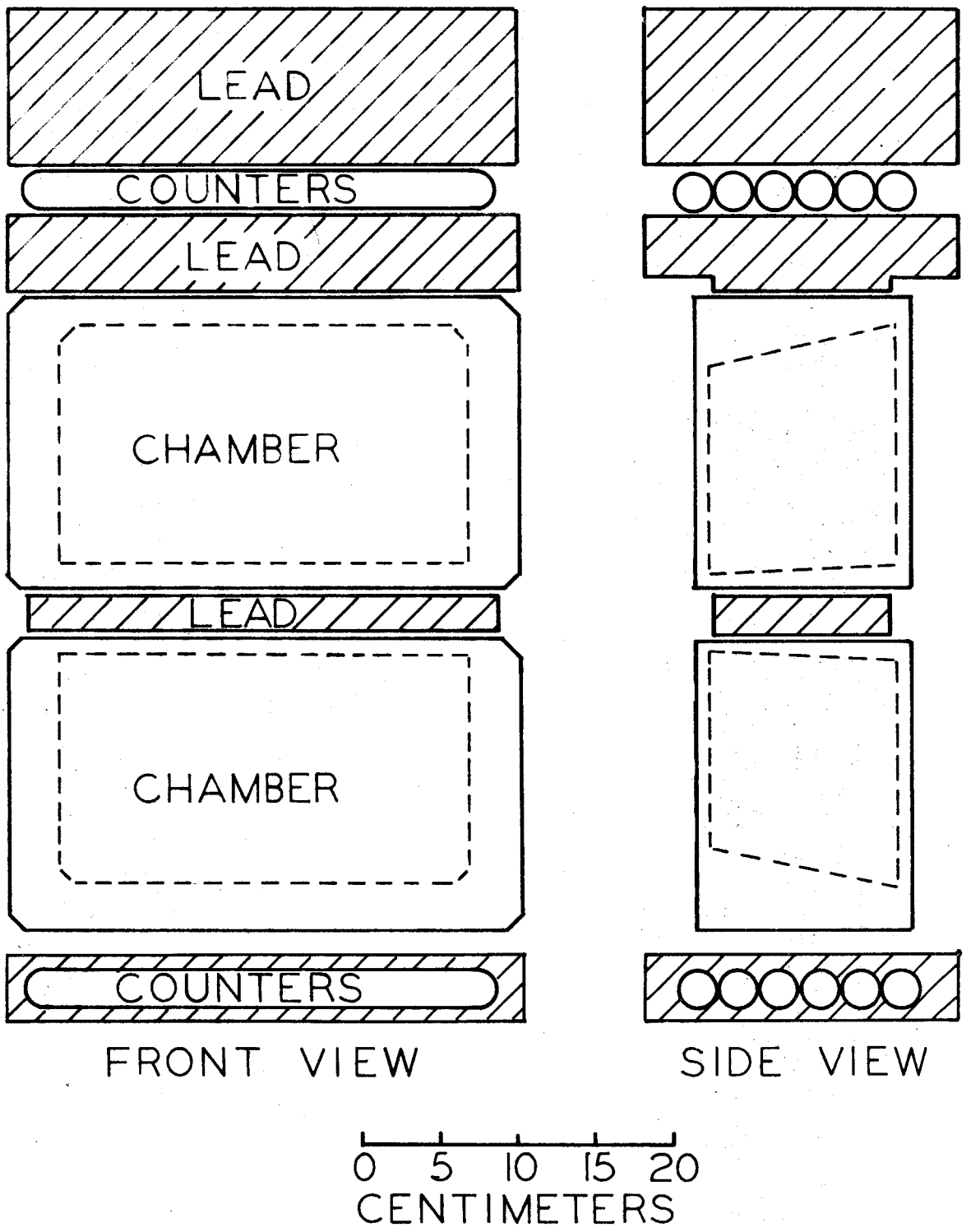

Fig. 1. The arrangement of counters and lead blocks around the cloud chambers. The dotted lines inside the chamber volume indicate the fiducial surfaces used in the lifetime study of Sec. 5. The magnet structure surrounding and supporting the apparatus is not shown.

the main responsibility of operation of the cloud chamber.

A program for the measurement of no-field tracks in order to determine the maximum detectable momentum was carried out. The magnetic field was turned off by a timing device for a period of 15 minutes every 3 hours. Shower particle tracks which penetrated the lead plate between the two chambers without multiplication and appreciable scattering were selected from photographs taken during this shut-off period. The curvatures were measured in exactly the same way as for tracks obtained with the magnetic field, and a histogram of the results was plotted. From the width of this distribution it has been concluded that the maximum detectable momentum for a track 15cm long is 3 Bev/c.

Several modifications were made in the thermostat system. Provision was made for recording the temperature variation of various parts of the chamber on the same film that was used to photograph the chamber. A study of these variations indicated that there was no observable change in the temperature conditions during the periods in which the magnetic field was turned off. This study also permitted a quantitative check on the gaseous distortions in the chamber. Considerable improvement in the temperature control was progressively attained, but because the events considered in this work were selected from the total operation period of the apparatus, one can only say that the short period temperature fluctuations of the cloud chambers were held to about $\pm$ 0.1^{o} C during the course of the work.

Various counter arrangements were used to trigger the apparatus. Of the 71,000 photographs taken of the cloud chamber, 14,000 were taken at 200 m elevation with a coincidence of one or more counters above the chamber and three or more below (this is called a 1-3 selection); 7,000 were taken with the same counter selection at 1750 m; 22,000 were taken at 1750 m with a 2-3 selection; and 28,000 were taken at 1750 m with 1-3 selection with lead shielding surrounding the lower counters. This shielding was accomplished by means of a cast lead block as shown in Fig. 1 and the counting rate with this arrangement was about 2.5/hr.

The momentum and angle measurements were made from the stereoscopic photographs in the same way as were those of Leighton et al.[14] Ionization estimates were in most cases made by three independent observers and a range of possible ionization assigned in the same manner used by the above authors; however, the method for measuring ionization photometrically, as described in Part I, was applied whenever possible.

3. The Data

The present analysis is based upon a total of 101 photographs of events which could be interpreted as charged V-particle decays, but not as pi-mu decays or scattering events.

Pi-mu decays: The well-known criteria derived from the dynamics of the pi-mu decay[4] were applied to each event, and events that could be interpreted as pi-mu decays were not included in the analysis. Because of the relatively high momenta and large

angles of decay of the charged V-particles, the relation $\sin\theta \leq \frac{40}{P}$, where θ is the angle between the line of flight of the secondary particle and the extension of the direction of the primary particle, and P is the primary momentum (in Mev/c), sufficed in most cases to distinguish the event from a pi-mu decay. Sixty-five cases were eliminated by the application of these criteria.

Scattering events: A reasonable criterion for distinguishing a charged V-particle decay from a scattering event has been to require that no blob of ionization be visible at the point of deflection for transverse momenta in excess of 75 Mev/c.[4] This has been considered a conservative estimate of the minimum transverse momentum P_T required to produce a visible recoil. And since no very clear basis for this estimate has been presented, a detailed study of photographs of scattering events in the chamber was made.* This study established as a criterion for distinguishing decays from scattering events: if an event for which $P_T \geqslant 50$ Mev/c gives rise to no observable cluster of droplets at the point of deflection, that event is almost surely not a scattering event. Only 8 cases were eliminated by the application of this criterion: 5 events with an observable recoil, and 3 events with $P_T \leqslant 50$ Mev/c.

Charged V-particles: Of the 101 events which were finally included in the analysis only nine were "completely" measurable in the sense that both momenta could be measured. An example of decay in this category is shown in Fig. 2. The momentum of either the primary or the secondary particle could be measured in forty-

---

* This work was initiated and carried out by Carl M. York, Jr.[6]

Fig. 2 Event No. 78113, which is listed in Tables IA and VIII. The heavily ionizing charged V-particle originates in the shower in the upper right-hand corner (A) and decays just above the lead plate separating the chambers. The secondary particle is ejected upward and to the left (B).

six cases. The data pertaining to these cases, including the nine "completely" measurable cases are given in Table IA. In twenty-eight cases neither momentum could be measured, but the sign of charge was determined. The data on these cases are presented in Table IB. The uncertainties quoted for the momenta (in both tables) were assigned taking into account: a) the error to be expected from multiple scattering (15), and b) an uncertainty whose size was appropriate to the length of track, and which was calculated using the maximum detectable momentum 3 Bev/c for a 15 cm track. The errors quoted for the measured ionization values are probable errors of measurements.

4. A Preliminary Survey of the Data

As stated above, only about one half of the events yielded a measure of the momentum of either the primary or secondary particle. However, some of the properties of charged V-particles can be investigated in the absence of these measurements, such as the distribution of decay points in the chambers, and the circumstances of the occurrence of the decay events.

4:1 Distribution of decay points

The first treatment of the data consisted of plotting the decay points of the charged V-particles inside the cloud chambers as shown in Fig. 3. In carrying out this scheme two very marked features were noted. First, the decay points were distributed very differently in the two chambers, there being a striking number

(1) Frame	(2) Origin & Sign	(3) P_1 (Mev/c)	(4) $(I/I_{min})_1$	(5) P_2 (Mev/c)	(6) $(I/I_{min})_2$	(7) θ	(8) P_T (Mev/c)	(9) x(cm)	(10) d(cm)	Remarks
7029	A(-)	185± 25	7.4±.06[a]	150± 20	1.3-2.0	85°	150± 20	11.5	13.2	
13484	P(+)	-	min.	100± 20	<1.7	41.°5	66± 15	5.5	15.0	
16347	A(-)	-	<1.5	<800	<1.5	11°	<150	12.8	16.0	Secondary through plate, 19° scatter
17620	A(-)	1050±470	<1.5	750+200	<1.5	8°	109± 28	3.8	15.5	
18194	A(+)	-	<1.5	180± 15	<1.5	39.°5	114± 10	3.4	16.2	Secondary through plate
19504	P(-)	-	<1.5	240± 20	1.3-2.0	48.°5	180± 15	1.5	12.8	
23329	P(+)	-	-	140± 10	<1.7	42°	94± 5	-	-	Heavy shower
25343	P(+)	185± 45	3.9±.05[a]	215± 43	<1.5	51°	165± 27	4.3	8.8	
26622	P(-)	-	1.5-2.5	295± 65	<1.5	33°	166± 35	5.4	14.7	
26801	P(-)	-	min.	170± 30	<1.5	42°	115± 20	4.9	14.0	Also V^o below
30201	P(+)	-	2-4	520± 75	2-4	18°	160± 40	1.1	14.6	Heavy secondary
30901	A(-)	-	min.	150± 20	<1.7	57°	125± 20	-	-	Primary through plate
31118	P(+)	-	-	260± 40	<1.7	53°	210± 30	-	-	
31134	A(-)	-	<1.5	345± 40	<1.5	20°	118± 20	0.5	12.3	
31589	P(-)	-	1.5-3.0	265± 40	<1.5	40°	170± 25	2.3	14.4	
31864	A(-)	-	min.	285± 45	min.	41°	182± 25	5.2	11.0	Also V^o

(1)	(2)	(3)	(4)	(5)	(6)	(7)	(8)	(9)	(10)	Remarks
32530	A(-)	465±220	1.6±.02[a]	590±250	<1.5	29°	285±120	6.4	14.7	
33124	A(-)	-	<1.5	262± 20	<1.7	70°	245± 20	1.7	4.4	
36726	A(+)	-	1.5-3.0	140± 30	<1.5	108°	135± 30	4.5	15.7	
36863	A(+)	-	<1.5	460±110	<1.5	23°	180± 40	4.0	15.7	
38688	P(+)	286± 30	2.6±.03[a]	-	1.3-2.0	55°	-	13.0	18.0	
39634	P(+)	-	<1.5	115± 10	<1.5	78°.5	113± 10	1.0	14.3	
40792	A(+)	-	<1.7	185± 40	<1.7	54°	150± 35	1.2	13.8	
40840	P(+)	95± 30	6-12	184± 20	<1.5	87.°5	184± 20	4.1	7.9	
41573	P(+)	-	<1.5	365± 50	<1.7	29°	175± 25	1.0	18.8	
41646	P(+)	-	3-7	320± 60	6.0-7.3[a]	20°	110± 25	0.9	18.3	Heavy secondary
42368	A(-)	245± 25	4.3±.02[a]	-	min.	128°	-	-	-	
43307	P(+)	-	min.	150± 15	<1.5	40°	98± 10	-	-	Heavy shower
43955	P(+)	-	min.	109± 10	1.5-3.0	81.°5	108± 10	-	-	
46613	A(+)	368± 40	2.3±.03[a]	-	min.	22.°5	-	-	-	
47214	A(+)	172± 15	7.5±.08[a]	-	<1.5	68°	-	12.1	13.9	
47332	A(-)	280± 90	< 2.5	-	1.3-2.0	89°	-	6.5	15.7	
48990	A(+)	-	<1.5	570± 90	<1.5	19.°5	190± 40	8.9	14.1	Secondary 7° scatter in plate
49169	A(+)	215±100	3.1±.02[a]	-	< 2	96°	-	3.9	14.0	

(1)	(2)	(3)	(4)	(5)	(6)	(7)	(8)	(9)	(10)	Remarks
50092	A(-)	-	<1.5	285± 45	<1.5	15°	75± 15	11.1	15.7	Secondary scatter in plate
50835	P(+)	-	min.	340± 40	<1.5	27°	155± 20	-	-	
52999	A(+)	165± 85	15-30	215± 60	1.3-2.0	121°	185± 50	2.5	6.2	
54056	P(-)	-	1.5-3.0	325± 75	<1.5	13°	73± 15	0.8	13.7	
55482	P(-)	-	1.5-2.5	182± 30	2-4	53.°5	146± 25	-	-	
55707	A(+)	230± 20	4.7±.06[a]	-	min.	38.°5	-	15.0	17.8	
58384	P(-)	780±350	<1.5	-	<1.5	40°	-	8.7	15.1	
59185	A(+)	-	min.	450±150	min.	21.°5	165± 60	6.4	14.9	
60452	A(+)	255±175	3.5±.07[a]	212± 10	<1.5	99°	210± 10	-	-	
60991	P(+)	-	<1.5	70± 5	1.5-3.0	55°	57± 4	1.3	14.1	
62894	P(+)	-	min.	300± 45	<1.5	88°	300± 45	-	-	
63350	A(-)	-	min.	70± 10	2-4	62°	62± 10	4.5	21.2	V^o from same origin
63469	P(-)	-	min.	360± 55	<1.5	29°	175± 25	-	-	
65550	A(-)	1500±800	<1.5	120± 50	<1.5	41.°5	79± 35	11.9	13.9	
66850	P(+)	-	min.	260± 55	<1.5	42°	175± 30	4.9	14.8	V^o from same origin
68007	P(+)	-	min.	325± 60	<1.5	32°	173± 30	3.8	15.0	
74491	P(-)	-	min.	95± 30	2-4	101°	92± 30	1.8	14.6	

(1)	(2)	(3)	(4)	(5)	(6)	(7)	(8)	(9)	(10)	Remarks
75617	A(-)	430± 90	< 2	-	-	79.°5	-	-	-	
77002	P(+)	-	min.	500± 60	<1.5	22°	187± 25	-	-	
77526	A(-)	-	min.	313± 30	< 2	44°	217± 20	-	-	
78113	A(+)	107± 15	10-15	251± 20	<1.5	133°	182± 15	-	-	

Table IA. Data on 46 cases with either primary or secondary momentum measurable and 9 cases with both momenta measurable. In column (2), A signifies an origin above the chamber and P an origin in the plate. The momenta and ionization of the primary particles are given in columns (3) and (4) and of the secondary in columns (5) and (6). The ionization values are visual estimates unless otherwise noted. The momenta were all computed from curvatures measured with a standard comparator. The angle θ, column (7), is the angle included between the direction of the secondary particle and the line of flight of the primary, measured from the stereoscopic projection. The decay lengths, column (9) and the potential path lengths, column (10), are also included.

[a] Ionization measured photometrically.

Frame	Origin & Sign	Primary (I/I_{min})	Secondary I/I_{min}	θ	x(cm)	d(cm	Remarks
22312	A(-)	min.	min.	32^{o}	-	-	π-μ decay also
23752	A(-)	<1.5	<1.5	10^{o}	9.2	15.5	
26340	P(-)	min.	<1.5	45^{o}	1.2	16.6	
26743	P(+)	min.	min.	25^{o}	7.4	15.5	
26912	A(-)	<1.5	<1.5	9^{o}	5.0	12.8	V^{-} origin of V^{o} below
27697	A(-)	min.	<1.5	12^{o}	3.5	14.8	
31886	P(+)	min.	min.	38^{o}	6.1	14.9	
36369	+	<1.5	<1.5	11^{o}	1.5	11.2	From star in glass
37753	A(-)	<1.5	<1.5	65^{o}	2.0	15.6	
39846	P(+)	<1.5	<1.5	11^{o}	4.8	14.6	
39955	A(-)	<2	min.	32^{o}	-	-	
42191	P(-)	<2	<1.5	26^{o}	-	-	Could come from plate
44420	P(+)	<1.5	<1.5	$7.^{o}5$	10.5	15.1	
49352	A(-)	min.	min.	$6.^{o}5$	-	-	Primary through plate
52207	P(+)	<1.5	<1.5	23^{o}	11.2	14.7	
53495	P(-)	min.	<1.5	98^{o}	-	-	
53590	P(+)	<1.5	<1.5	18^{o}	3.0	12.9	

54606	A(-)	<1.5	1.5	16^{o}	11.8	15.7	
57072	A(-)	min.	min.	13^{o}	-	-	Primary through plate
57541	A(+)	<2	min.	61^{o}	2.5	17.5	
57791	A(-)	<2	<2	60^{o}	8.8	23.2	
60043	A(-)	<1.5	<1.5	62^{o}	-	-	
61249	P(+)	<1.5	<1.5	43^{o}	10.1	13.5	
63816	A(-)	min.	min.	24^{o}	5.9	16.6	
66958	A(-)	min.	min.	31^{o}	7.7	15.7	
75546	P(+)	<1.5	min.	69^{o}	2.1	16.5	
77166	P(+)	<1.5	<1.5	30^{o}	-	-	
77946	P(-)	min.	min.	63^{o}	-	-	V^{o} from same origin

Table IB. Date on 28 cases with momenta not measurable, but sign of charge determined.

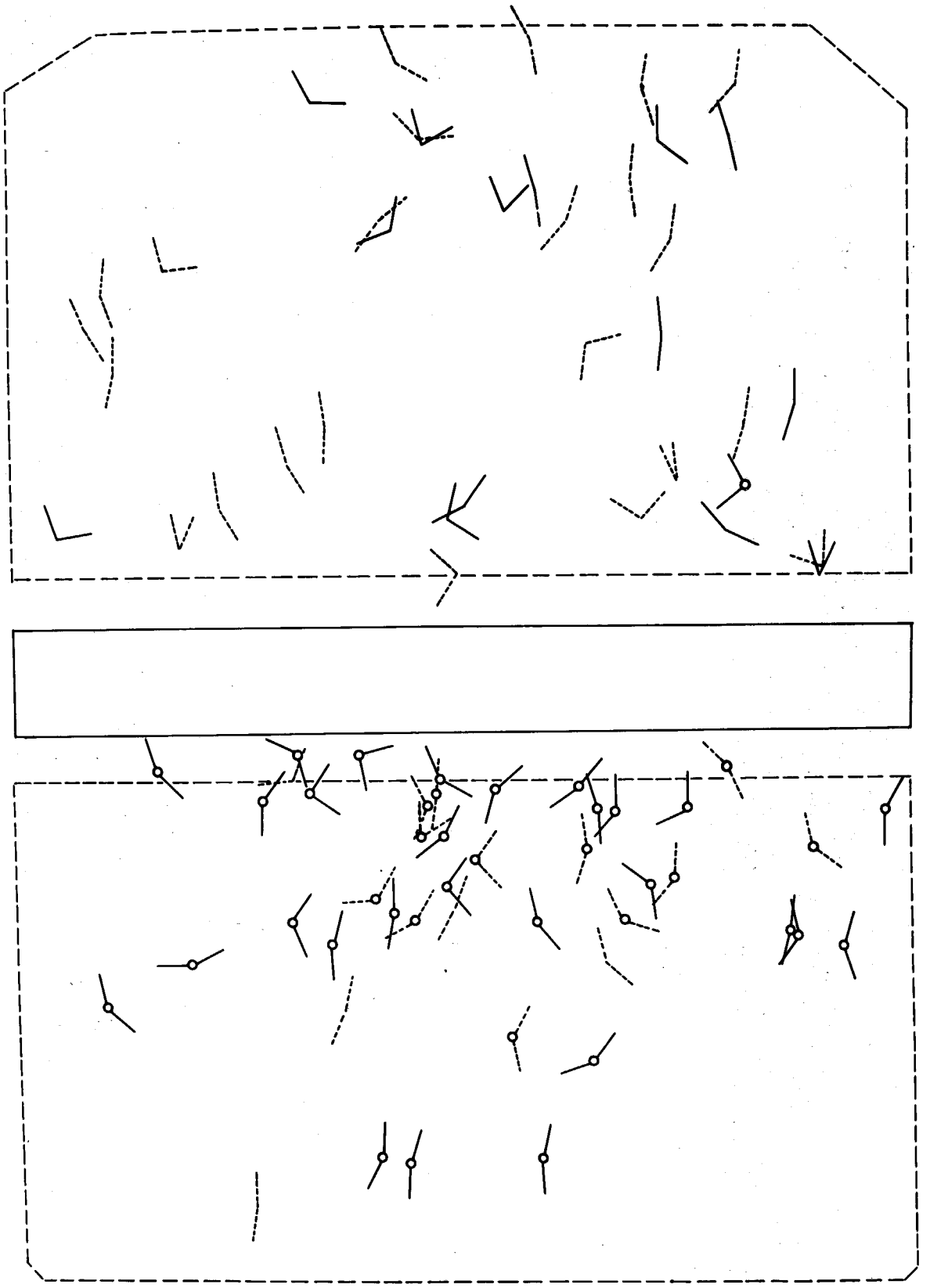

Fig. 3. The distribution of the charged V-particle decay points. A circle at the apex indicates production in the lead plate separating the two chambers. Solid lines indicate positive particles and dashed lines indicate negatives.

of very short decay lengths in the lower chamber, and second, the charge ratio of the decaying particles was found to be quite different in the two chambers. A convenient way to indicate the asymmetry of charge is set forth in Table II where the number of positively and negatively charged V-particles with origins above the chambers or in the lead plate separating the two chambers is given. A table of this form has previously been published,[12] and the numbers have simply been brought up to date in the present version. It is of interest to calculate the statistical probability that the observed sample, having this charge asymmetry, could have been obtained from a population with no charge asymmetry. * Let $(N^+)a$ and $(N^-)a$ be the number of positive and negative particles, respectively, in the upper chamber, and $(N^+)p$ and $(N^-)p$ the corresponding numbers in the lower chamber. Then the most probable composition (of positive and negative particles) of the population, on the basis of the two samples (upper and lower chamber) is:

$$p(\text{positive}) = \frac{(N^+)a + (N^+)p}{Na + Np} \quad , \quad q(\text{negative}) = 1-p \tag{1}$$

where $Na = (N^+)a + (N^-)a$ and $Np = (N^+)p + (N^-)p$. The standard deviation, σ of p can be written,

$$\sigma^2 = pq\left[\frac{1}{Na} + \frac{1}{Np}\right] , \tag{2}$$

and the observed charge asymmetry can be expressed,

---

*Dr. R. P. Dilworth has kindly suggested the procedure for this calculation.

$$\Delta = \frac{(N^+)a}{Na} - \frac{(N^+)p}{Np} \quad . \tag{3}$$

The ratio $\frac{\Delta}{\sigma}$ is then a measure of the likelihood of the observed degree of asymmetry, and the probability of obtaining an asymmetry as great as or greater than $\frac{\Delta}{\sigma}$ can be read from a standard table. The probability was found to be 0.002 using the observed numbers. And, since p = 0.50, this is then the probability that the charge asymmetry would be obtained as a fluctuation from a uniform charge distribution in the two chambers.

These marked asymmetries have already been tentatively interpreted in terms of a mixture of long and short-lived charged V-particles.[6] By considering the relative positions of the production layer and the cloud chamber, the charged V-particles observed in the upper chamber were presumed to be predominantly long-lived particles with a negative excess of about two to one at their point of production. (This need not imply that a single type of particle is observed, but only that the particles are predominantly long-lived.) The charged V decays in the lower chamber are then supposedly a mixture of both long and short-lived particles and should be predominantly if not entirely positively charged.

4:2 Search for associated γ-rays:

A careful survey of the data was made for possible evidence of the existence of γ-rays associated with the decay of charged V-particles.[7] One might expect to see electron cascades generated in the lead block between the chambers; however, in no case was such a cascade observed. It should be noted that

Origin	Charge pos. (N^+)	neg. (N^-)	$\frac{N^+}{N^-}$
above chamber	14	28	$0.50 \pm .16$
plate between chambers	28	13	$2.15 \pm .65$
Total	42	41	1.02

Table II. Classification of charged V-particle decays according to their sign of charge and place of origin. The errors quoted for N^+/N^- are probable errors.

Type of event	$V^{\pm}$	V^o	$R(V^{\pm}/V^o)$
Charged primary, accompanied by other shower particles	27	83	0.32 ± 0.07
Charged primary, unaccompanied	10	21	0.48 ± 0.19
Neutral primary, (acc. and unacc.)	5	14	0.36 ± 0.18
Totals	42	118	0.36 ± 0.05

Table III. The number of penetrating shower particles occurring in the lead plate between the chambers giving rise to $V^{\pm}$ - particles, classified according to the type of primary. Similar data for neutral V-particles are included and the ratio R, $(V^{\pm}/V^o)$ calculated for each category. The errors quoted for R are probable errors.

this does not imply that there are no γ-rays among the decay products of the charged V-particles, because the thickness of the lead block (about six radiation lengths) makes it a very inefficient detector for low energy cascade showers.

4:3 Mechanism of production:

In order to study the mechanism of production of charged V-particles it is convenient to classify them according to the circumstances of their occurrence: forty were found in penetrating showers with origins in the lead above the chambers, forty-two were produced in nuclear inter-actions in the lead plate between the chambers, and twenty were not clearly associated with any event. The forty-two events originating in the lead plate were further classified according to the nature of the primary particle initiating the event. The result is summarized in Table III. It is seen that most of the events were produced by particles which were themselves secondaries of penetrating showers. A similar classification of data taken with the same apparatus and over the same period of time has been made of 118 neutral V-particles and these results are included in the Table. The striking similarity of the two sets of numbers indicates that the charged V-particles originating in the lead plate are produced by a mechanism as similar to that of neutral V-particles, and that meson-nuclear collision in lead can give rise to charged V-particles. A similar result has been obtained at the Brookhaven Laboratory where artificially produced pi-mesons have bombarded hydrogen to produce charged V-particles.[16] Leighton et al.,[14] on the basis of their data,

conclude that, although nucleon-nuclear production is possible, the majority of their neutral V-particles were produced in meson-nuclear collisions. Furthermore the constancy of the ratio of charged to neutral V-particles in each category, within the limits of the statistics, suggest that the charged V-particles in the lower chamber are produced with about one-third the frequency of neutral V-particles, independently of the nature of the producing particle. The frequency of production of charged V-particles will be discussed in more detail in Section 6 in connection with the life-time analysis.

It is also of interest to compare the number of particles produced above the chamber and in the plate, for both the neutral and charged V-particles. The results are shown in Table IV. Similar numbers for penetrating showers are also included in the table. In the work of Leighton et al. the neutral V-particles produced in penetrating showers above the chamber apparently did not show any characteristics different from the particles produced in the plate. So in view of the similarity noted above, of the types of events occurring in the plate that produce neutral and charged V-particles, this result seems to indicate that the charged V-particles found in penetrating showers above are not produced by the same mechanism as are those from the plate, or that the particles above are predominantly of another type.

The question as to whether or not V-particles are produced in pairs can also be investigated by these preliminary methods. Leighton et al. find that the neutral V-particles are probably not produced in pairs. The present data are in agreement with this conclusion. Nine double events were found, all consisting of a

Type of particle	Produced above (N_a)	Produced in plate (N_p)	$R\left(\frac{N_a}{N_p}\right)$
$V^{\pm}$	40	43	0.93
V^{o}	279	118	2.36
Penetrating shower particles	1060*	250*	4.23

Table IV. The number of charged and neutral V-particles produced in the lead above the chamber and in the plate. Similar data for penetrating shower particles are included and the ratio R (N, above/N, plate), calculated for each group.

* Counts from rolls of film representative of the various counter selections.

neutral V^o (the nature of which could not be determined) and a charged V-particle: five of these pairs had their point of production in the plate between the chambers. Another two pairs were also produced in the plate, but the particles could not have originated at the same point.

5. Lifetimes

The preliminary treatment of the data above suggested that two or more types of charged V-particle with a marked difference in lifetimes and sign of charge might exist. The evidence relating to the lifetimes will now be considered in detail.

The necessity for obtaining a sufficiently large, unbiased sample of V-particle decays of a single type, in order to determine their mean life with any precision, limits the use of cloud chamber observations unless a definite classification of the particles can be made. The present data do not, in most cases, distinguish between the possible types of charged V-particles. However, limiting values of the mean life, τ, of any given set of charged V decays can be made which do not involve a detailed knowledge of the nature of the particles observed. It is important to stress that the limiting lifetimes thus obtained may refer to an unknown mixture of two or more types of particles, but that even in such a case it may still be possible to obtain meaningful limits upon the lifetimes of the constituents of such a mixture.

5:1 Reduction of the data

The method used in the reduction of the data was essentially the same as that used by Alford and Leighton.[17] The same fiducial surfaces were employed (Fig. 1). The minimum requirements of determination of the sign of charge and the existence of an approximate origin were satisfied for 83 charged V events at the time the analysis was carried out. Of these, 62 cases had their point of decay inside the fiducial surfaces. The rather large fraction, 26 percent, excluded by the fiducial limits can be compared to the 14 percent of the neutral V-particles similarly excluded by Alford and Leighton. Most of the excluded charged V-events are near the front glass or back piston of the chamber where neutral V-particles are difficult to identify.

The experimental quantities which were used in this analysis are as follows: x_i is the distance (in cm.) between the point of entrance of the i^{th} particle into the region of the chamber inside the fiducial limits and the point of decay. D_i is the corresponding distance (in cm.) between the point of entrance and the point at which the particle would have left the fiducial region had it not decayed. D_i is usually called the gate length. t_i and T_i are the times taken to traverse the distance x_i and D_i, respectively, in the rest system of the V-particle. These proper times are related to the measured distances by the equation

$$t_i = (x/c)(M/P_i c) = (x_i/c)\,(1/\beta_i \gamma_i) \qquad (4)$$

where M is the mass of the particle in Mev and P_i is the measured momentum in Mev/c. A similar relation can be written for T_i. The quantities c, β, and γ have the usual significance.

In each case it is necessary to have an estimate of $\beta_i\gamma_i$, and if the particle has a known mass and measurable momentum, this product is easily obtained. However, since one rarely knows these two quantities, an alternate procedure must be employed. In practice, the ionization of a particle is a function of velocity alone (provided the charge of the particle is not in question). In most cases it is possible to determine upper and/or lower limits to the ionization, and therefore estimates of $\beta_i\gamma_i$ can be obtained.

In all but four of the 62 cases was it possible to assign an upper limit to the ionization of the primary particle. A measurement of the ionization, by the method described in Part I, was possible in only nine of these cases. In 39 of the remaining cases the ionization was indistinguishable from minimum, and in these cases the upper limit was taken to be one and one-half times minimum. These upper limits determined lower limits to $\beta_i\gamma_i$ in each case and by means of Eqn. (4) upper limits to t_i and T_i.

On the other hand, the sign of charge, as determined from the direction of curvature of the parent particle, was in all cases the same as that obtained from that of the secondary particle, which had easily measured momenta. Thus the momenta of the primary particles themselves were presumably within the upper limit set by the chamber distortions, so that this limit, 3Bev/c, could be used as an upper limit to the momentum of each primary particle. Taking the mass of the primary particles as 1000 m_e (or greater) the upper momentum limit thus obtained gave a lower limit to t_i and T_i.

Although this latter method is useful, its limitations should be emphasized. If the sample of decay events being treated is predominantly of one sign of charge, as is the case in the present application, and if the chamber has a small, systematic gas distortion of a type which appears as a smooth curve, then the estimates of the sign of charge of the primary particle might easily be biased to give better agreement with the true sign of charge than would have been obtained in the absence of the distortion. If such were the case, the maximum detectable momentum might no longer be a conservative estimate of the upper limit to the momentum of the V-particle. It is clear that such a bias will be more important for short tracks near the edges of the chamber than for long tracks near the center. Thus the interpretation of any results obtained with this method must be carried out with due caution.

In order to treat the whole sample uniformly, only the two methods just described were used to establish limits to t_i and T_i, including 14 cases for which the momentum of the primary particle was measurable. This procedure has advantages in that it does not bias the sample by the selection of slow particles with long tracks for which the momentum is readily measurable, and it permits most of the observed cases to be included in the analysis. The data on the 58 cases finally included in the lifetime analysis thus consist of two sets of values of t_i and T_i corresponding to an upper and lower limit to each and are presented in Tables V,A and B. Of the 30 cases in the lower chamber, four negative particles apparently had their origin in the lead above the upper chamber, but were treated in this analysis as if they originated in the

plate between the chambers. In Table VI the number of cases observed in each chamber, the average limiting values of t and T, the average value of x/D, and the ratio of the number of positive to the number of negative particles in each chamber are given. The distribution of x/D for the two chambers is shown in Figs. 4 and 5. These data show the marked difference between the two chambers and the necessity for treating each chamber separately. It is seen that the limiting values of $\overline{T}$ for the two chambers are very nearly the same. This would be expected for identical chambers, provided no bias due to the selection of groups of particles with greatly different average velocities has been introduced.

5:2 Upper chamber:

For gate times which are small compared to the mean life-time of the decaying particles, one expects the decay points to be uniformly distributed throughout the chamber, and hence the average value of x/D to be equal to one-half. It is immediately apparent from Table VI that such is the case in the upper chamber, so that the "apparent" lifetime of the decaying particles in the upper chamber is probably much greater than the average gate time, viz.

$$\tau \text{ (upper chamber)} > 4.5 \pm 1.6 \times 10^{-10} \text{ sec.}$$

The statistical estimation of mean lifetimes has been discussed in detail by Bartlett.[18] It seems that his method can be used with advantage to make a more precise statement about the mean life, although no finite estimate of τ is possible.

(1) Frame	(2) Sign	(3) x(cm)	(4) d(cm)	(5) x/d	(6) I/I_{min}	(7) $t_U(10^{-10}sec)$	(8) $t_L(10^{-10}sec)$	(9) $T_U(10^{-10}sec)$	(10) $T_L(10^{-10}sec)$
7029	-	11.5	13.2	0.87	6.8-8.0[a]	13.7	10.6	15.8	12.3
16347	-	12.8	16.0	0.80	1.5	3.9	1.0	4.8	1.3
18194	+	3.4	16.2	0.21	1.5	0.6	0.4	3.0	2.1
23752	-	9.2	15.5	0.60	1.5	2.8	0.8	4.7	1.3
26912	-	5.0	12.8	0.39	1.5	1.5	0.4	3.9	1.1
27697	-	3.5	14.8	0.24	min.	0.7	0.3	3.1	1.2
31134	-	0.5	12.3	0.04	1.5	0.2	0.0	3.7	1.0
31864	-	5.2	11.0	0.47	min.	1.1	0.5	2.3	0.9
33124	-	1.7	4.4	0.39	1.5	0.5	0.1	1.3	0.4
36726	+	4.5	15.7	0.29	1.5-3.0	4.0	1.4	9.0	4.8
36863	+	4.0	15.7	0.25	1.5	1.2	0.3	4.8	1.3
37753	-	2.0	15.6	0.13	1.5	0.6	0.2	4.7	1.3
40792	+	1.2	13.8	0.52	1.7	1.4	0.4	2.8	0.7
47214	+	12.1	13.9	0.87	6.7-8.3[a]	11.2	12.9	7.0	8.0
47332	-	6.5	15.7	0.41	2.5	3.3	2.0	9.0	4.8
48990	+	8.9	14.1	0.63	1.5	2.7	0.7	4.3	1.2
49169	+	3.9	14.0	0.28	$3.1 \pm .02$[a]	2.5	1.4	9.0	4.9

(1)	(2)	(3)	(4)	(5)	(6)	(7)	(8)	(9)	(10)
50092	-	11.1	15.7	0.71	1.5	3.4	0.9	4.8	1.3
52999	+	2.5	6.2	0.40	15-30	4.9	3.0	12.2	7.4
54606	-	11.8	15.7	0.75	1.5	3.6	1.1	4.8	1.4
55707	+	15.0	17.8	0.84	4.7±.06[a]	13.9	8.6	16.5	10.2
57541	+	2.5	17.5	0.14	2	0.8	0.2	5.4	1.5
57791	-	8.8	23.2	0.38	2	3.7	1.9	9.7	4.9
59185	+	6.4	14.9	0.43	min.	1.3	0.5	3.1	1.2
63350	-	4.5	21.2	0.21	min.	0.9	0.4	4.4	1.8
63816	-	5.9	16.6	0.35	min.	1.2	0.5	3.5	1.4
65550	-	11.9	13.9	0.86	1.5	2.5	2.9	1.0	1.2
66958	-	7.7	15.7	0.49	min.	2.3	0.7	4.8	1.4

Table VA. Data on 28 cases with origin above the chambers for which the decay length x and the potential path length d could be measured. t and T are decay time and gate-time (with respect to the center-of-mass system of the particle), and the subscripts refer to upper and lower limits, calculated as described in the text.

[a] Ionization measured photometrically.

(1) Frame	(2) Sign	(3) x(cm)	(4) d(cm)	(5) x/d	(6) I/I_{min}	(7) $t_U(10^{-10}sec)$	(8) $t_L(10^{-10}sec)$	(9) $T_U(10^{-10}sec)$	(10) $T_L(10^{-10}sec)$
13484	+	5.5	15.0	0.36	min.	1.1	0.3	3.0	0.8
17620	-	3.8	15.5	0.25	1.5	1.2	0.3	4.6	1.3
19504	-	1.5	12.8	0.12	1.5	0.5	0.2	3.9	1.4
25343	+	4.3	8.8	0.49	$3.9\pm.05$[a]	2.2	1.3	4.4	2.7
26340	-	1.2	16.6	0.07	min.	0.3	0.1	3.5	0.9
26622	-	5.4	14.7	0.37	1.5-2.5	2.7	1.6	7.3	4.4
26743	+	7.4	15.5	0.48	min.	1.9	0.5	3.3	0.8
26801	-	4.9	14.0	0.35	min.	1.5	0.4	4.2	1.0
30201	+	1.1	14.6	0.08	2-4	0.6	0.2	2.5	0.8
31589	-	2.3	14.4	0.16	1.5-3.0	1.3	0.7	8.3	4.5
31886	+	6.1	14.9		min.	1.3	0.3	3.1	0.8
32530	-	6.4	14.7	0.44	1.5	1.9	0.5	4.4	1.2
36369	+	1.5	11.2	0.13	1.5	0.5	0.2	3.6	1.3
38688	+	13.0	18.0	0.72	$2.6\pm.03$[a]	6.6	3.9	9.1	5.5
39634	+	1.0	14.3	0.07	1.5	0.1	0.0	3.0	0.8
39864	+	4.8	14.6	0.33	1.5	1.5	0.5	4.6	1.6

(1)	(2)	(3)	(4)	(5)	(6)	(7)	(8)	(9)	(10)
40840	+	4.1	7.9	0.52	6-12	5.7	3.8	11.0	7.3
41573	+	1.0	18.8	0.05	min.	0.3	0.1	5.7	2.1
41646	+	0.9	18.3	0.04	3-7	1.1	0.7	22.0	14.9
44420	+	10.5	15.1	0.70	1.5	3.2	1.1	4.6	1.6
52207	+	11.2	14.7	0.76	1.5	4.7	1.2	6.1	1.5
53590	+	3.0	12.9	0.23	1.5	0.9	0.3	3.9	1.4
54056	-	0.8	13.7	0.06	1.5-3.0	0.5	0.2	7.9	4.2
58384	-	8.7	15.1	0.58	1.5	2.6	0.7	4.5	1.3
60991	+	1.3	14.1	0.09	1.5	0.4	0.1	4.3	1.6
61249	+	10.1	13.5	0.75	1.5	3.0	1.1	4.1	1.4
66850	+	4.9	14.8	0.33	min.	1.0	0.3	3.1	0.8
68007	+	3.8	15.0	0.25	min.	0.8	0.2	3.1	0.8
74491	-	1.8	14.6	0.12	min.	0.5	0.2	4.4	1.5
75546	+	2.1	16.5	0.13	1.5	0.4	0.1	3.4	0.9

Table VB. Data on 30 cases with origin in the plate between the chambers for which the decay length x, and the potential path length d could be measured. t and T are decay time and gate time (with respect to the center-of-mass system of the particle), and the subscripts refer to upper and lower limits, calculated as described in the text.

[a] Ionization measured photometrically.

	No. of cases	$r = \frac{N^+}{N^-}$ [a]	$(x/D)_{Av.}$ [b]	$\bar{t}$ (10^{-10} secs)		$\bar{T}$(10^{-10} secs)	
				upper limit	lower limit	upper limit	lower limit
Upper Chamber	28	0.65 ± 0.25	0.46 ± 0.10	3.2	1.5	6.1	2.9
Lower Chamber	30	2.00 ± 0.77	0.31 ± 0.09	1.7	0.8	5.4	2.4

Table VI . Comparison of the events used in the lifetime study. r is the ratio of positive to negative particles, $(x/D)_{av}$ is the average value of the ratio of decay length to gate length, t is the average time of flight in the chamber before decay, and $\bar{T}$ is the average gate time.

a. The errors quoted for r are probable errors.
b. The errors quoted for $(x/D)_{av}$ are 95 percent confidence limits.

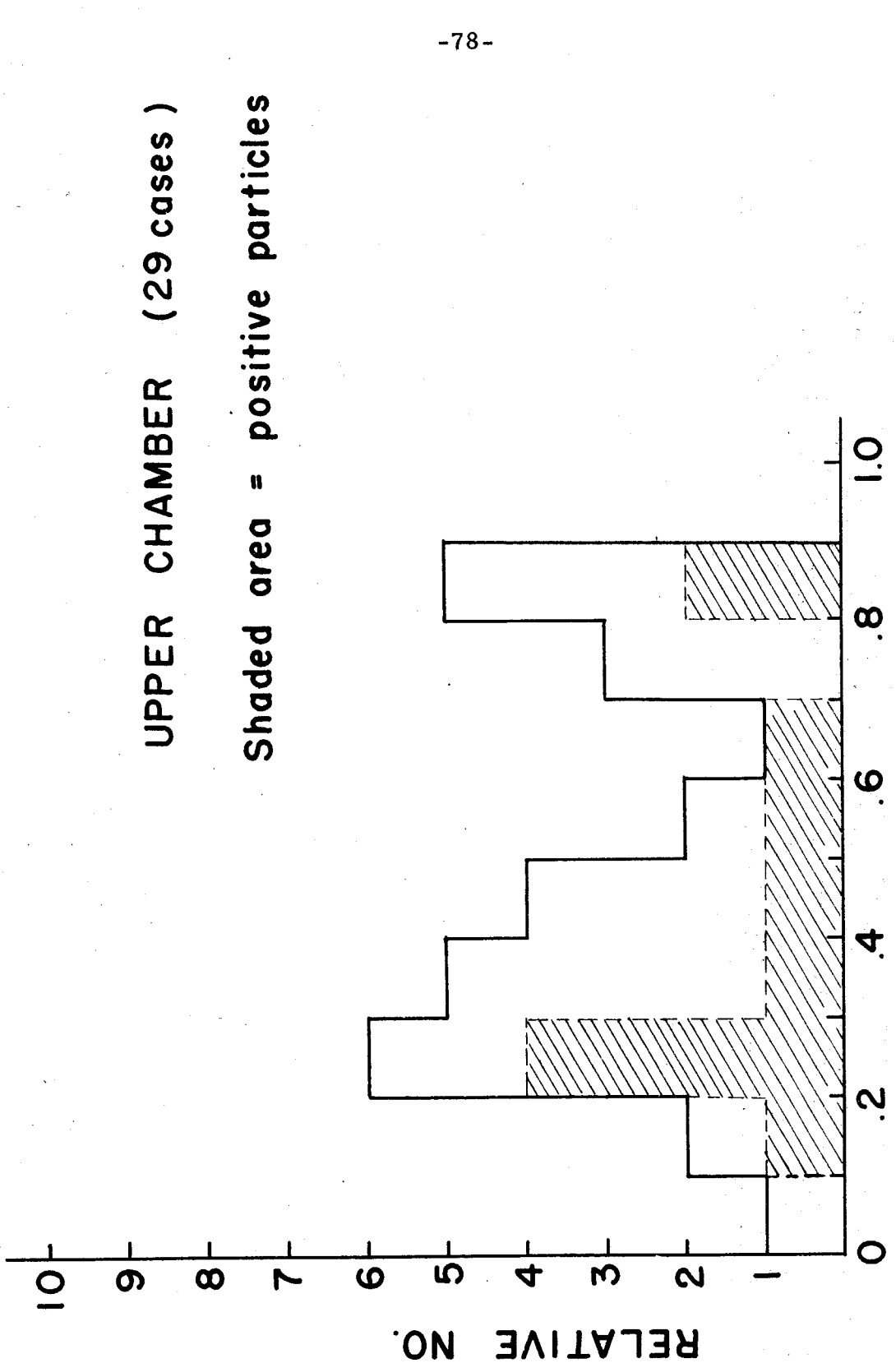

Fig. 4. The distribution of x/D for the upper chamber.

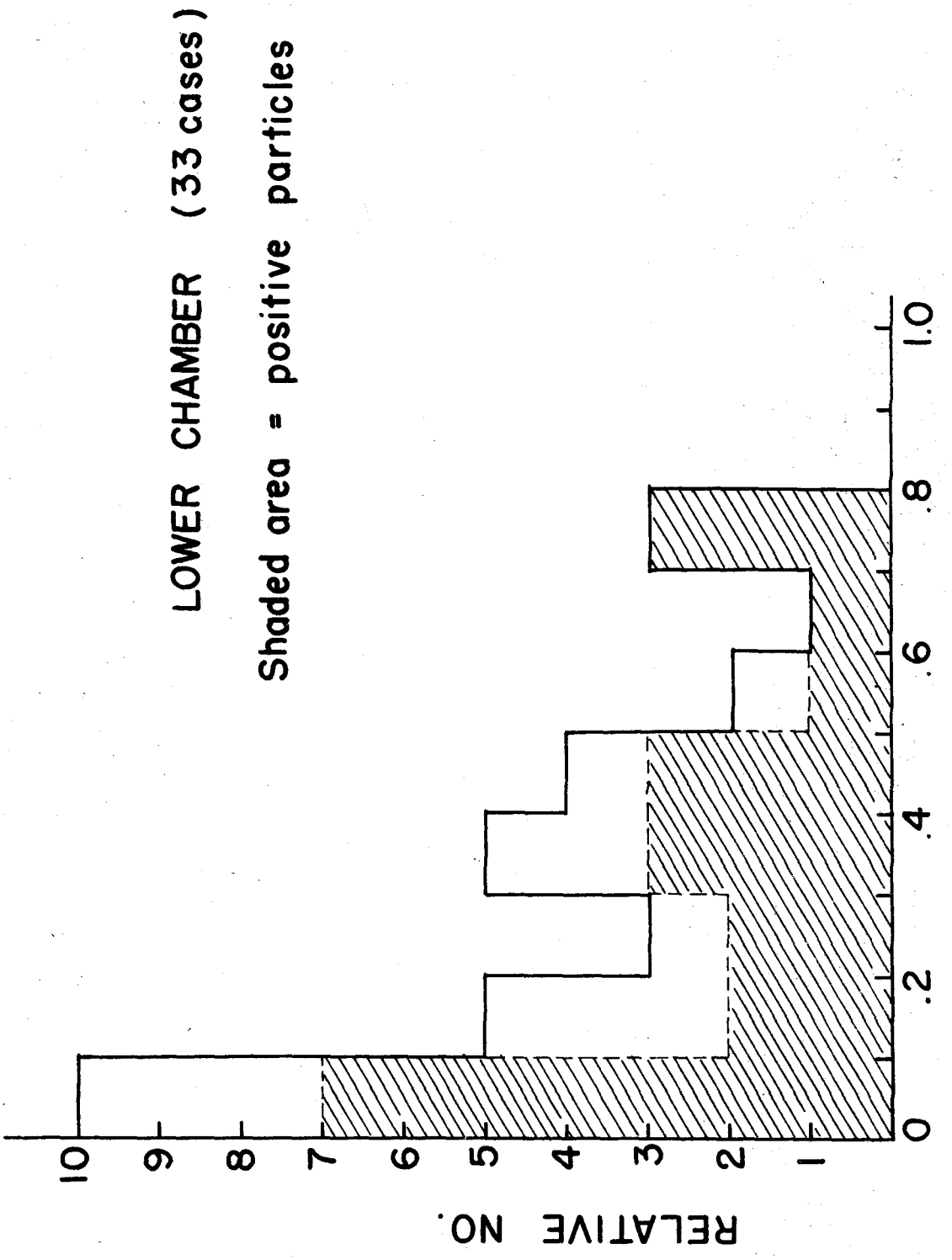

Fig. 5. The distribution of x/D for the lower chamber.

The likelihood function

$$L = \prod_{i=1}^{N} \frac{1}{\tau} \frac{\exp(-t_i/\tau)}{1-\exp(-T_i/\tau)} \tag{5}$$

is proportional to the probability of having obtained the particular set of experimental data. The best value of the parameter τ is that value which makes L (or more conveniently $\ell n\, L$) a maximum:

$$f(\tau) = \frac{\partial \ell n\, L}{\partial \tau} = \frac{1}{\tau} \sum_{i=1}^{n} \left[\frac{t_i}{\tau} - 1 + \frac{T_i}{\tau} \left(\frac{\exp -T_i/\tau}{1-\exp -T_i/\tau} \right) \right] = 0 \tag{6}$$

Bartlett then considers the standardized quantity

$$S(\tau) = \frac{\sum_{i=1}^{n} \left[\frac{t_i}{\tau} - 1 + \frac{T_i}{\tau} \left(\frac{\exp -T_i/\tau}{1-\exp -T_i/\tau} \right) \right]}{\left\{ \sum_{i=1}^{n} \left[1 - \left(\frac{T_i}{\tau} \right)^2 \frac{\exp -T_i/\tau}{(1-\exp -T_i/\tau)^2} \right] \right\}^{1/2}} \tag{7}$$

which has zero mean and unit variance, and is obtained from Eqn. (6) by dividing $f(\tau)$ by the statistical variance of $f(\tau)$. By treating $S(\tau)$ as a normal (Gaussian) distribution it is possible to obtain confidence limits on τ corresponding to any probability level. From a graph of $S(\tau)$ against τ (or $1/\tau$) the confidence limits may be read off by equating $S(\tau)$ to the associated value derived from the normal distribution and corresponding to the chosen probability level. In Fig. 6 the values obtained for $S(\tau)$ are plotted against $1/\tau$, and a probability level of 95 percent $[S(\tau) = 1.645]$ is indicated. It is apparent from the graph that the value $1/\tau = 0$ is quite consistent with the data, and that no upper limit can be assigned to

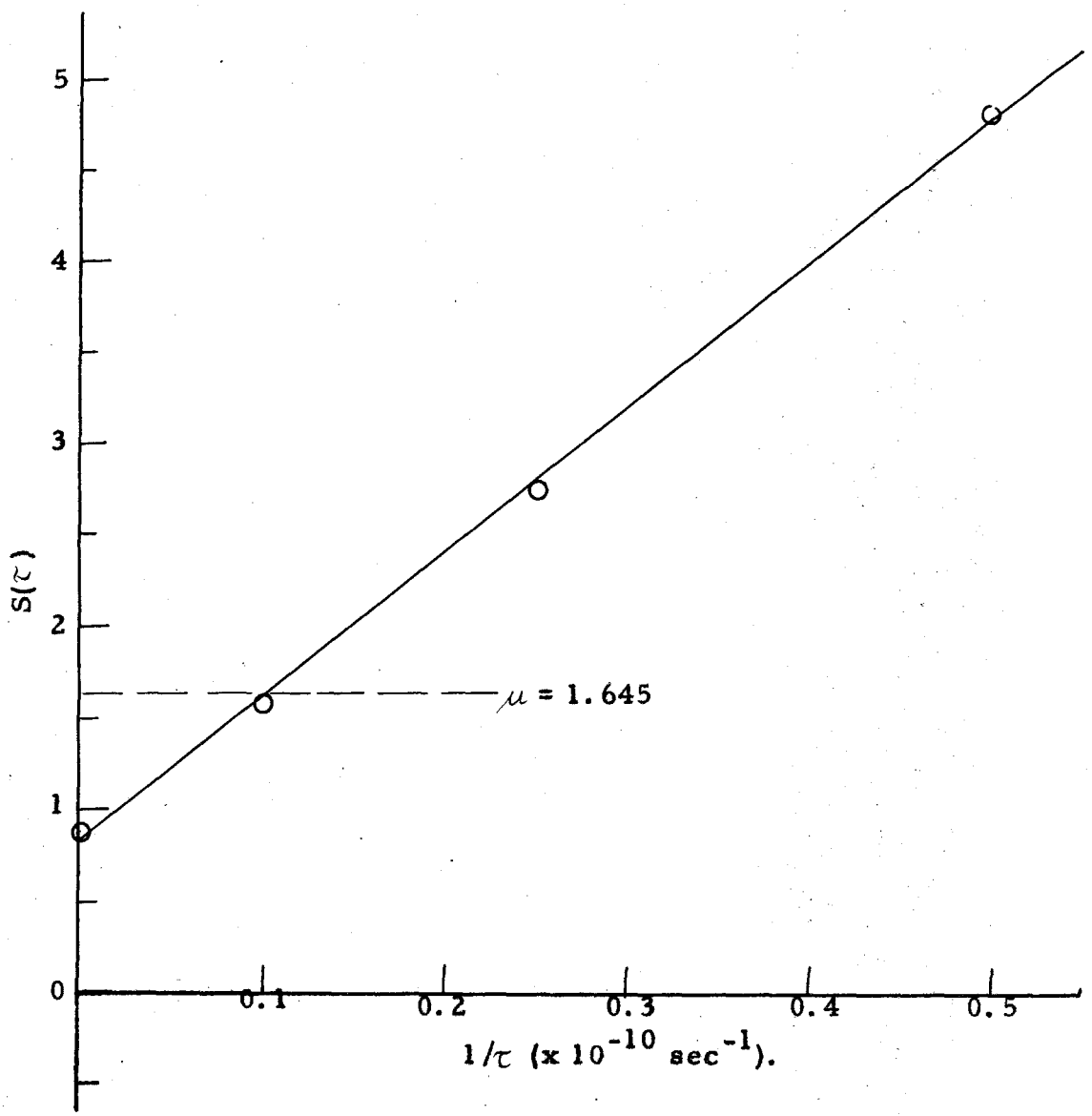

Figure 6. A plot of the function $S(\tau)$ vs. $1/\tau$ (Eqn. 7) for the data of the upper chamber. The value of $S(\tau)$ for a probability level of 95 per cent is indicated.

the lifetime. However, it is possible to establish a lower limit to τ, on the 95 percent probability level:

$$\tau \text{ (upper chamber)} > 10^{-9} \text{ sec.}$$

That these events do not necessarily represent a single type of particle is indicated by the fact that one negative case in this chamber could be identified as a cascade decay such as those recently reported. A careful search was made for additional cases where a neutral V-particle might have decayed in the plate, but none was found.

5:3 Lower chamber:

For the sample of 30 cases in the lower chamber the average ratio (x/D) is significantly different from 0.50, as is shown by conventional statistical methods. The error assigned to the value quoted in Table VI, $(x/D)_{av} = 0.31 \pm 0.09$, has been computed using the "Student" distribution with a probability level of 95 percent.[19] In other words, the probability that $(x/D)_{av}$ exceeds 0.40 is less than 0.05. Therefore a maximum likelihood analysis[17,18] has been made to determine limiting values on τ.

The best value of the mean life (that value of τ for which L (Eqn. 5) is a maximum) is given by:

$$\tau = \frac{1}{N} \sum_{i=1}^{N} \left[t_i + \frac{T_i}{\exp(T_i/\tau) - 1} \right] \qquad (8)$$

By expanding the exponential function in the parentheses, this can be written in a form more convenient for the calculation of τ :

$$\tau = \frac{\sum_{i=1}^{N} T_i^2 - \frac{1}{60}\tau^{-2}\sum_{i-1}^{N} T_i^4 + \cdots}{6\sum_{i=1}^{N} T_i - 12\sum_{i=1}^{N} t_i} \qquad (9)$$

The calculation of τ for the two limiting sets of data gives, using Eqn. (5):

$$\tau \text{ (upper limit)} = 2.77 \times 10^{-10} \text{ sec.}$$

$$\tau \text{ (lower limit)} = 1.49 \times 10^{-10} \text{ sec.}$$

Bartlett[18] has shown that if t_i and T_i are consistently overestimated, each by the same factor a_i, then the best value of τ determined from the likelihood function is correspondingly an overestimate of the lifetime of the sample, and similarly for underestimates. The calculation of the likelihood function, L (Eqn. 5), was performed for seven values of τ to determine the significance of these limits, and the results are shown in Fig. 7. The ordinates of the curves were normalized to the value of L for $\tau \to \infty$, i.e.;

$$L \simeq \prod_{i=1}^{N} \left(\frac{1}{T_i}\right) \text{ as } \tau \to \infty \qquad (6)$$

It is seen that the likelihood function has a very pronounced maximum for both sets of data, the peak values being 121 and 46 times that for $L(\tau \to \infty)$ for the upper and lower limit of τ respectively. But in order to estimate the probable errors for these limiting values of the mean lifetime, the probability that $\tau \leq \tau_o$ must be calculated. This probability, $F(\tau_o)$ is given by the integral $F(\tau_o) = \int_o^{\tau_o} L(\tau)\, d\tau$. The integration can be performed graphically

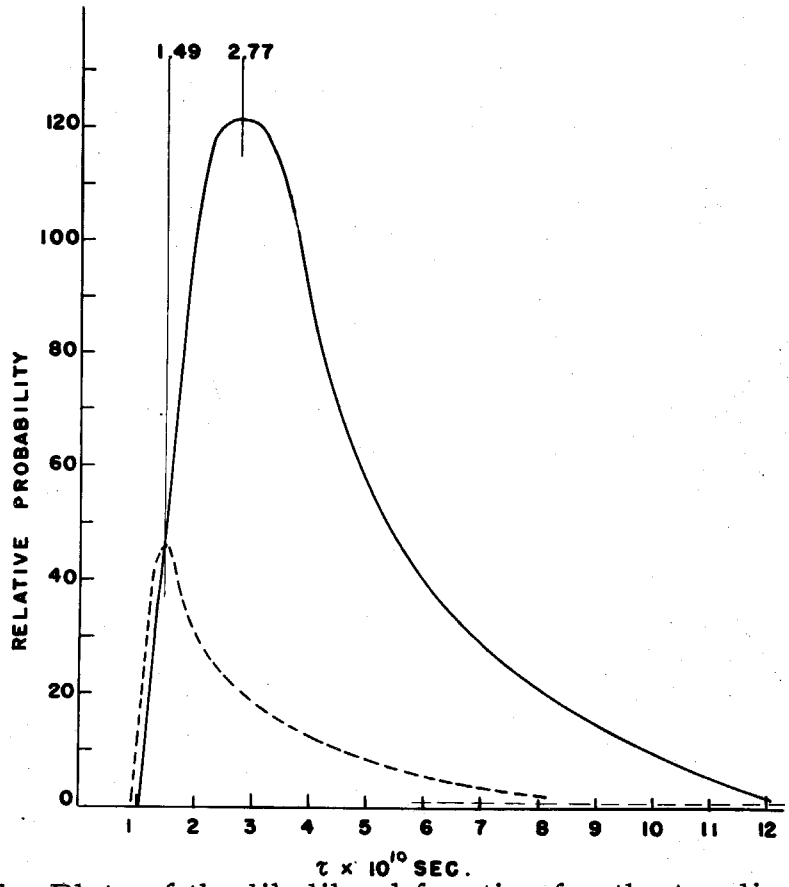

Fig. 7. Plots of the likelihood function for the two limiting lifetime estimates obtained from the data of the lower chamber. The solid curve is for the estimate of the upper limit and the dashed curve for the lower limit of the mean life.

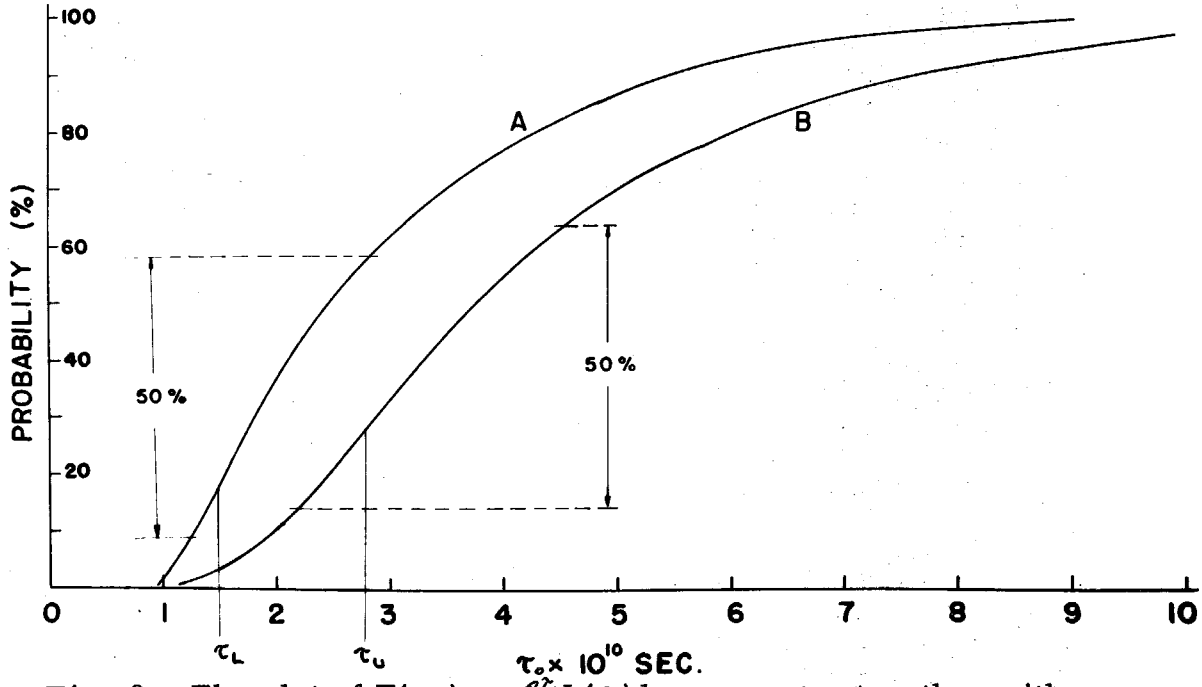

Fig. 8. The plot of $F(\tau_0) = \int_0^{\tau_0} L(\tau)d\tau$ versus τ_0, together with the assigned 50 percent confidence limits to each of the limiting estimates of the lifetime found in the lower chamber.

and the resulting curves are given in Fig. 8. As indicated in the figure, 50 percent confidence limits have been used to determine the probable errors on the two limiting values of the mean lifetime. The result is:

$$1.5\begin{cases}+1.3\\-0.3\end{cases} < \tau < 2.8\begin{cases}+2.0\\-0.6\end{cases} \quad \times 10^{-10} \text{ sec.}$$

These limits can be associated with the mean life of a specific particle only if the sample is composed entirely of particles of that type. If the sample is pure, then these limits indicate that the particle has a lifetime between them. If the sample is a mixture of particles, then the upper limit indicates that at least one type of particle with lifetime less than 2.8×10^{-10} sec. is contained in the sample and the lower limit implies that another type of particle with lifetime greater than 1.5×10^{-10} sec. is present. However, in view of the earlier remarks about possible bias in the determination of this lower limit, no very great significance should be attached to it.

6. Additional Properties of Charged V-Particles

In addition to the lifetimes discussed in the previous section, several other measured properties of charged V-particles deserve some detailed consideration. These are: (1) the nature of the particles involved in the decay, (2) the distribution of the transverse momenta of the secondary particles, and (3) the value of the momentum p* of the secondary particle in the center-of-mass system of the decay. Because the lifetime study showed a

marked difference in the charged V's decaying in the upper and lower chambers, it seems reasonable to investigate the remaining decay properties by analyzing the events in the two chambers separately to bring out any further differences.

6:1 Masses of charged V-particles and their decay products.

The nature of the primary particles can in part be inferred from measurements of momentum and ionization. Masses determined in this way for charged V-particles are given in Table VII. Only cases for which a measurement of the ionization as described in Part I could be obtained are included. In the cases for which it was not possible to measure the ionization of the particles with any accuracy, previously obtained visual estimates were used, and a frequency distribution of the mass values is plotted in Fig. 9. The measurable cases are also included in this plot, but only visual estimates of the ionization were used to calculate the masses. The results for the secondary particles are also shown.

It can be concluded that the masses of the primary particles are in agreement with a mass of about 1000 m_e. However, it should be noted that the requirements of measurability demand that the particles travel a considerable distance at low velocity before decaying, so that any sample of such mass measurements will be strongly biased in favor of particles with long mean lives. It is interesting that of the fourteen heavily ionizing, measurable primaries contained in the data all except three are observed in the upper chamber and contribute to the long mean lifetime observed there. As mentioned above, four negative particles were

Frame No.	Sign and Origin	P(Mev/c)	I/I_{min}	$M(m_e)$
7029	A(-)	185 ± 20	7.4 ± 0.6	1140 ± 150
25343	P(+)	185 ± 60	3.9 ± 0.5	770 ± 320
32530	A(-)	465 ± 100	1.63 ± 0.2	930 ± 210
38688	P(+)	286 ± 30	2.55 ± 0.3	860 ± 120
42368	A(-)	245 ± 15	4.30 ± 0.3	1080 ± 100
46613	A(+)	368 ± 30	2.25 ± 0.3	990 ± 110
47214	A(+)	172 ± 15	7.50 ± 0.8	1070 ± 120
49169	A(+)	215 ±100	3.05 ± 0.2	750 ± 350
55707	A(+)	230 ± 15	4.65 ± 0.3	1080 ± 100
60452	A(+)	255 ± 60	3.60 ± 0.4	990 ± 250

Table VII. Data on 10 cases with measurable primary momentum and measured ionization. The errors quoted for the masses have been computed from the combined errors of measurement.

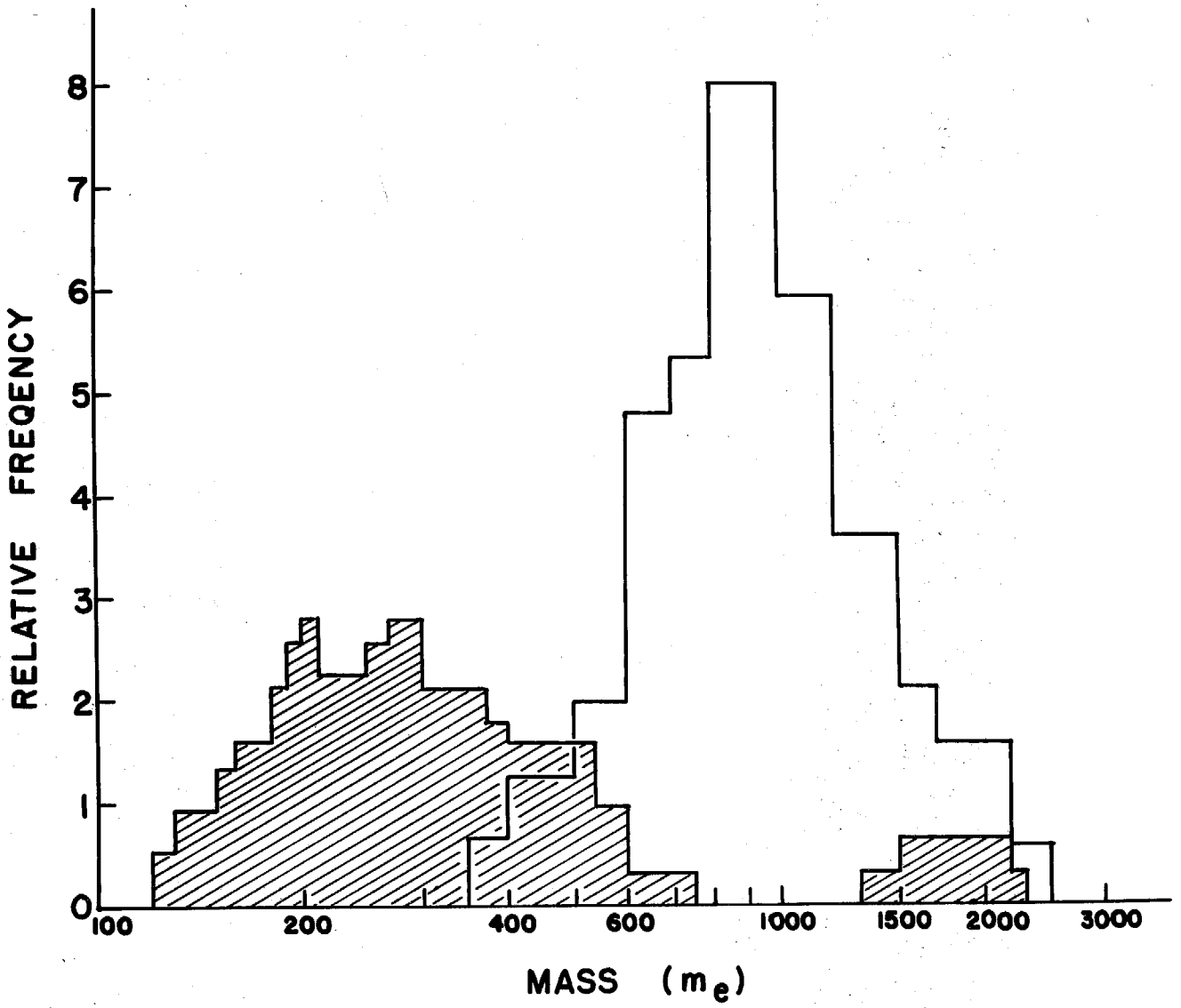

Fig. 9. Frequency distribution of the measured masses. The unshaded area gives the masses of the primary particles and the shaded area the masses of the secondaries. Ten positive and seven negative primaries are represented.

observed to traverse the lead plate between the chambers before decaying, but these give no information regarding the nuclear interaction of the particles because it would not have been possible to identify a star in the plate produced by a charged V-particle.

In Fig. 9, it is seen that the masses of all except two of the secondary particles are consistent with either that of a π or μ-meson. The two exceptions will be treated in detail in the section below. No secondary particle was observed to decay in flight, and only four traversed the lead plate separating the chambers. None of the secondary particles produced a nuclear interaction and therefore no conclusion can be drawn with regard to whether these were π or μ-mesons.

6:2 The distribution of transverse momentum.

In considering the transverse momentum distribution of the secondary particles emitted in charged V-particle decay, the data from the upper and lower chambers have been treated separately. The resulting distributions are given in Figs. 10 and 11. Here the number of cases per 50 Mev/c interval is plotted against the transverse momentum. The shaded areas indicate the contribution of positive particles to the total distributions. In accord with the minimum transverse-momentum criterion required to eliminate π-μ decays and scattering events, these distributions do not have any cases with p_T less than 50 Mev/c. The smooth curves represent the calculated distributions for two and three-body decay with fifteen percent experimental errors folded in. The three-body decay curve has been calculated by assuming that a 1000 m_e primary particle (K-meson) decays into a mu meson

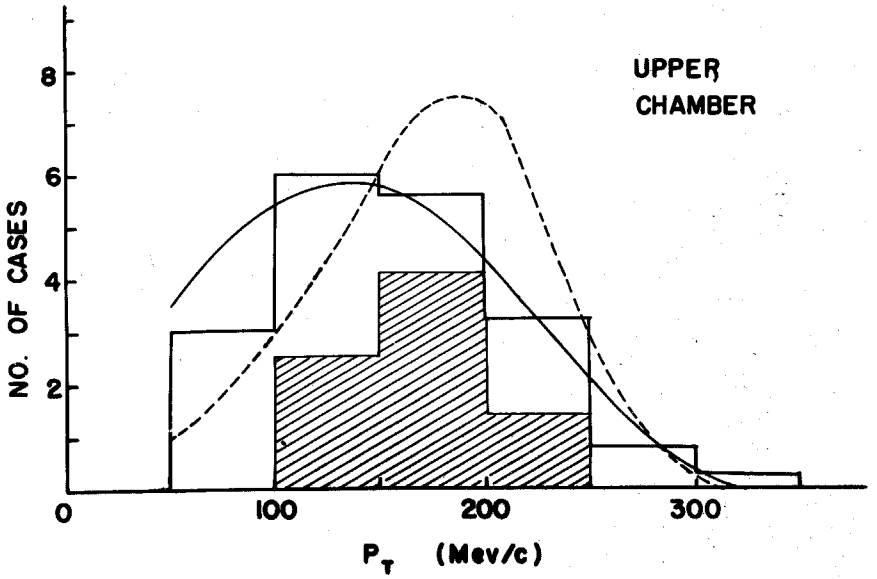

Fig. 11. Frequency distribution of transverse momenta.

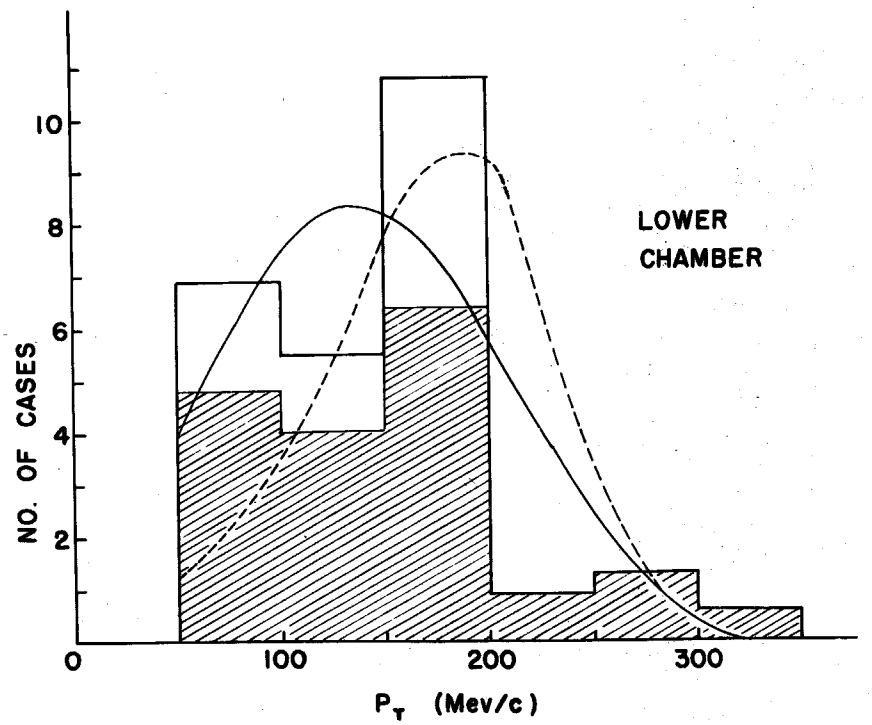

Fig. 10. Frequency distributions of transverse momenta. The shaded areas indicate the contribution of positive particles in the total distribution. The solid curve is calculated for a three-body decay (p* = 240 Mev/c) and the dashed curve for a two-body decay (p* = 216 Mev/c).

and two zero-rest-mass particles, and that the matrix element of the interaction is independent of the energies of the particles produced in the decay.[20] The two-body curve has been calculated for a momentum of the charged meson of 216 Mev/c in the center-of-mass system of the decay.[4] This value of the momentum is that assumed for chi meson decay[9] and has been plotted for ease of comparison. The areas under the curves for $p_T < 50$ Mev/c have been normalized to be equal to the total areas contained in the frequency distributions of the experimental data. *

By cutting off the distributions at 50 Mev/c, bias of the data is reduced due to contamination from scattering events as well as due to the difficulty of observing low transverse momentum cases. It is clear that such cases will in general involve small angles of deflection which might easily be overlooked in searching through the film for charged V-events. Because the transverse momentum depends upon the measurability of the momentum of the secondary particle, the distributions of transverse momentum will be slightly biased to include more of the short-lived primary particles than of the longer-lived ones. However, a relatively inconsequential bias will result and the small amount of data does not warrant a correction for this effect.

Because there are relatively few cases involved in these distributions, it is not possible to make significant statistical tests of the "goodness of fit" of the theoretical curves and the

---

* This work was performed by Dr. C. M. York.

experimental data. It is clear that many more cases would be needed to distinguish clearly between two and three-body decay schemes. On the other hand, although the level of statistical significance is low, the transverse momentum distributions in the two chambers would appear to indicate some differences in the type of decay involved.

6:3 The distribution of momentum in the center-of-mass system.

In treating the determination of the momentum, p*, of the secondary particle in the center-of-mass system, care has been taken not to introduce any bias into the data. All cases in which the primary particle was judged to be heavily ionizing and the transverse momentum of the secondary was measurable are listed in Table VIII. The limits of ionization of the primary particle were used to obtain the limits on the velocity of the center-of-mass system of the decay. By applying a Lorentz transformation to the longitudinal component of momentum of the secondary particle the corresponding limits to the longitudinal component of p* were obtained, and combining these limits with the errors of measurement of p_T the final limits to p* were determined. For completeness several cases in which the primary particle was essentially at minimum ionization but had a measurable momentum are included. These cases are indicated in the table and p* has been calculated for them by assuming that the primary particle has a mass of 1000 m_e.

The small number of cases and the errors inherent in the observations preclude any detailed interpretation of the values of p*; however, the spread of values, especially in the upper

Frame No.	Origin and Sign	P_1(Mev/c)	$(I/I_{min})_1$	P_2(Mev/c)	$(I/I_{min})_2$	θ	P_T(Mev/c)	P^*(Mev/c)
7029	A(-)	185± 25	6.8-8.0[a]	150± 20	1.3-2.0	85°	150± 20	125-190
17620	A(-)	1050±470	1.5	750±200	1.5	8°	109± 28	179± 40[b]
25343	P(+)	185± 45	3.4-4.4[a]	215± 43	1.5	51°	165± 27	130-210
26622	P(-)	-	1.5-2.5	295± 65	1.5	33°	160± 35	130-210
31589	P(-)	-	1.5-3.0	265± 40	1.5	40°	170± 25	150-210
32530	A(-)	465±220	1.4-1.8[a]	590±250	1.5	29°	285±120	316±120[b]
36726	A(+)	-	1.5-3.0	140± 30	1.5	108°	135± 30	180-320
40840	P(+)	95± 30	6-12	184± 20	1.5	87.°5	184± 20	170-220
52999	A(+)	165± 85	15-30	215± 60	1.3-2.0	121°	185± 50	180-290
54056	P(-)	-	1.5-3.0	325± 75	1.5	13°	73± 15	100-190
55482	P(-)	-	1.5-2.5	182± 30	2-4	53.°5	146± 25	125-210
60452	A(+)	255±175	2.8-4.2[a]	212± 10	1.5	99°	210± 10	220-255
65550	A(-)	1500±800	1.5	120± 50	1.5	41.°5	79± 35	213± 50[b]
78113	A(+)	107± 15	10-15	251± 20	1.5	133°	182± 15	280-325

Table VIII. Data on 9 cases with both momenta measurable and 5 cases with primary ionization 1.5 x min and secondary momentum measurable.

[a]Ionization measured photometrically. [b]P^* calculated assuming a mass of 1000 m_e for the primary particle.

chamber, seems to favor a non-unique value of p*. This could result from either a mixture of several types of two-body decay, or from a single three-body scheme. In particular, the distribution is completely consistent with what might be expected for K-meson decay.

7. The Frequency of Production of Charged V-Particles

The frequency of production of charged V-particles relative to neutral V-particles occurring in the lower chamber has been discussed in Section 4:3. It is also of interest to calculate the frequency of production relative to the total number of shower particles.* This has been carried out for the two chambers separately, using a method similar to that of Barker et al.[21] The geometry used in this experiment is shown in Fig. 1 . In the lower chamber, only production in the lead block separating the two chambers has been considered. In calculating the curves shown in Fig. 12 it has been assumed a) that particles of unique mass are observed to decay in each chamber, b) that all of the shower particles have a differential momentum distribution of the form $P^{-3}dP$ for momenta in excess of 1 Bev/c, c) that the penetrating showers are produced uniformly throughout the production layer, and d) that the cross-section for penetrating shower production is insensitive to the energy of the primary particles. For

---

* This calculation was suggested by Dr. C. M. York, who also helped to carry it out.

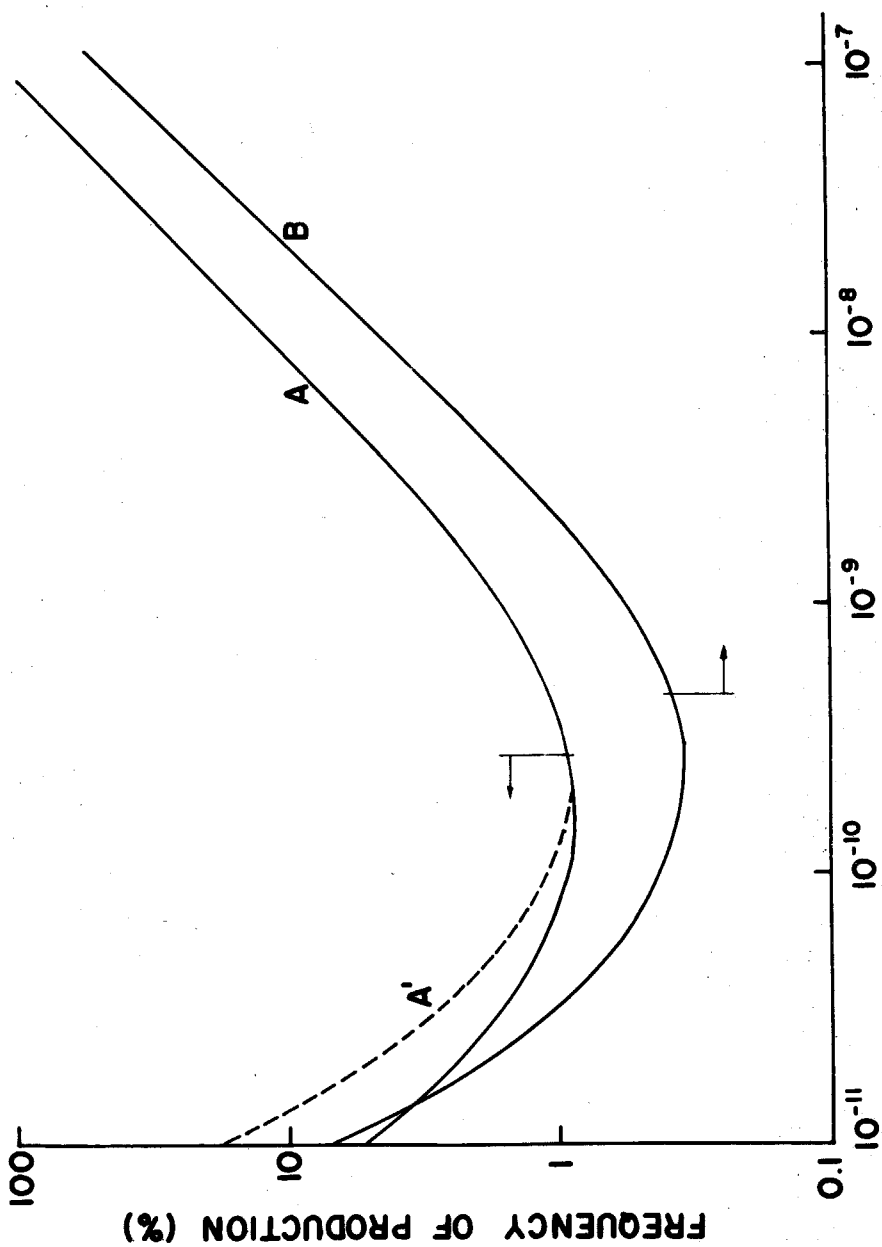

Fig. 12. The frequency of production vs lifetime curves for the upper chamber (curve B) and the lower chamber (curve A). The dashed curve, A', is calculated for the lower chamber assuming a mass of $2000m_e$. The lines with arrows attached, which intersect the curves, indicate the limiting lifetimes obtained in Sec. 5.

simplicity it is also assumed e) that all of the shower particles and decaying charged V-particles travel vertically downward. If the detection efficiency as a function of the lifetime of the decaying particles is evaluated using the above assumptions, the frequency of production as a function of the lifetime can then be obtained from the observed ratio of decaying V-particles to the total number of shower particles. From 1045 counted shower particles with momenta above 1 Bev/c, a weighted total of 35,600 particles produced in the lead block above the upper chamber and 8,400 produced in the lead between the chambers were estimated to have been seen during the course of the experiment. These are to be compared to 41 charged V's with momenta greater than 1 Bev/c observed in the upper chamber and 43 in the lower. The resulting curves of the frequency of production as a function of the mean lifetime are plotted in Fig. 12. For both curves a mass of 1000 m_e for the decaying particles has been assumed, but the dotted line A's lying just above the curve for the lower chamber has been calculated assuming a mass of 2000 m_e to show the small effect of this assumption. The vertical lines in the figure indicate the limits on the mean lifetimes estimated in Section 5 and the attached arrows indicate the range in which the true mean lifetimes for the two groups of particles probably lie.

The particles in the lower chamber have a frequency of production which is insensitive to the lifetime for a fairly large range of values of the lifetime. An estimate of the lower limit to the lifetime of these particles can be obtained by assuming that their frequency at production is ten percent of all of the shower

particles. This gives a lower limit of about 10^{-11} sec. If this same criterion of ten percent is applied to the upper chamber, one can estimate an upper limit to the lifetime of the particles decaying there of about 2×10^{-8} sec.

8. The Charged Hyperon. (V_1^+)

In the previous sections several marked differences in the decay properties of the charged V-particles in the upper and lower chambers have been noted. One of these differences which was briefly mentioned in the discussion of the masses of the secondary particles in Section 6:1 above, is that two charged V-particles having secondary particles with masses much greater than that of the π-meson were found in the lower chamber, both being positive and both having origins in the lead plate separating the two chambers. In both cases the primary track was too short to permit a momentum measurement, but was heavily ionizing. The secondary particles have masses lying in the range 1300-2300 m_e. It should be emphasized that while these heavy secondaries are quite consistent in mass and charge with protons, the mass measurements do not exclude the possibility that they are somewhat lighter and heavier than protons. A tentative interpretation of these events as being examples of the decay of a charged counterpart of the familiar V_1^o-particle has already been made[12]. The pertinent data for these two cases are contained in Table IX, and a photograph of one of the cases is reproduced in Fig. 13. The possibility that these events might be interpreted as the scattering of protons is ruled out by the

Frame No.	P_1 (Mev/c)	$(I/I_{min})_1$	M_1 (m_e)	P_2 (Mev/c)	$(I/I_{min})_2$	M_2 (m_e)	θ	P_T (Mev/c)
30201	-	2-4	-	520±75	2-4	1800±500	18°	160±40
41646	-	3-7	-	320±60	6.0-7.3[a]	1860±400	20°	110±25

Table IX. Summary of the data pertaining to the two cases of V_1^+ decay.

[a] Ionization measured photometrically.

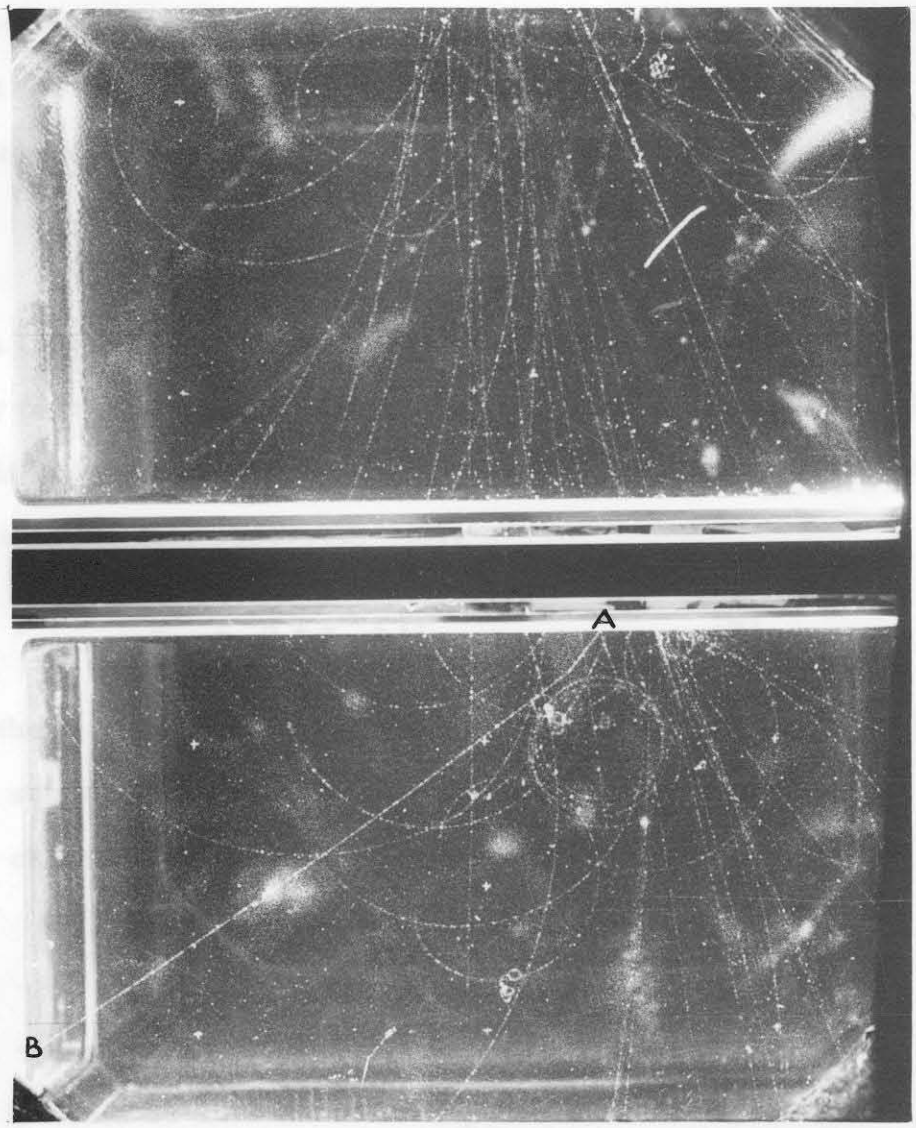

Fig. 13. Event No. 41646, showing a charged V-particle originating in an interaction in the lead plate and decaying into a heavy secondary particle. The V-particle travels diagonally downward toward the left from the interaction (A) and decays after having traversed only a short distance in the chamber. The secondary particle (B) proceeds almost in the same direction as the V-particle. Both the primary and the secondary particles are heavily ionizing.

high transverse momentum of the decay and the absence of a recoil nucleus at the decay point*. It is natural to suggest that this new decay follows the decay scheme;

$$V_1^+ \ (\text{or} \Lambda^+) \rightarrow p + \pi^o + Q \qquad (A)$$

Because a large number of the short-lived particles give rise to secondary particles whose masses are consistent with that of light mesons, it is inferred that the charge-exchange counterpart of the above reaction is also observed, viz.;

$$V_1^+ \rightarrow n + \pi^+ + Q \qquad (B)$$

Although there is no direct evidence in the present data, it is possible that some of the short-lived negative particles observed in the lower chamber represent the decay scheme;

$$V_1^- \rightarrow n + \pi^- + Q \qquad (C)$$

However, without accurate estimates of the masses of the primary particles it would be difficult to distinguish these two types of decays from that of a K particle in any individual case.

---

* This interpretation and the possibility that they may represent V^o-decays was investigated in detail by Dr. C. M. York, who found that neither interpretation could be considered satisfactory[6].

9. Conclusions

From the analysis of the data obtained in the two cloud chambers, it seems quite likely that the charged V-particles observed in this experiment are composed of at least two types with quite different properties. The events in the upper chamber appear to be predominantly due to a particle of mass about $1000m_e$ which decays into a light meson with a mean lifetime greater than 10^{-9} sec and less than 2×10^{-8} sec. A study of the transverse momentum and momentum in the center-of-mass system of the secondary particle indicates that there is probably more than one additional neutral particle involved in the decay. From a consideration of the maximum value of the transverse momentum and the rest mass of the primary particle it seems likely that these neutral particles are of very small rest mass and presumably are neutrinos and/or photons. The frequency of production of these particles is greater than 0.4 per cent of the total number of shower particles. The properties of these V-particles are in every respect consistent with those of the kappa meson,[8] and similar in every way to the properties deduced from earlier cloud chamber work employing a similar geometric arrangement of the apparatus.[4, 21]

However, recently published results on charged V-particles[22-26] (exclusive of hyperons) appear to be at variance with the properties of the previously postulated kappa and chi mesons. Other decay schemes have therefore been proposed to explain the experimental evidence. Gregory et al.[22] can explain the majority of their data by the decay scheme:

$$K_{\mu}^{\pm} \rightarrow \mu^{\pm} + \nu + Q$$

with $Q \simeq 360$ Mev ($P_{\mu} \simeq 220$ Mev/c), $M_{K_{\mu}} = 914 \pm 20 m_e$ and lifetime of the order of 3×10^{-8} sec. Almost complete absence of negative primaries is found. Evidence for this process appears to be present in the work of Kim et al.[24]* A very marked charge asymmetry is also found by these authors: a positively charged, longlived particle possibly decaying according to the above decay scheme, and a negatively charged, short-lived particle with a probable three-body decay process. The properties of the charged V-particles observed in the upper chamber in the present experiment are not compatible with the above results. This disagreement is not easily explained on the basis of the presently accepted decay processes of charged V-particles. It is possible that the geometric arrangement of the various apparatus used to detect V-particles introduce important bias in the selection of events.

The events in the lower chamber have a mean lifetime of less than 3×10^{-10} sec. Although several of the events in this chamber are probably kappa mesons, as indicated by mass measurements on the primaries, some other much shorter-lived particle must predominate to give such a low upper limit to the mean life of the sample. This particle appears to decay most of the time into a light meson and to be predominantly positive. The transverse momentum distribution indicates that probably a two-body decay occurs with a momentum in the center-of-mass system of about

---

* The author is indebted to Dr. Thompson for sending a prepublication copy of this paper.

200 Mev/c or less for the secondary particles. The frequency of production of these events is equal to or greater than about 0.8 per cent of the total number of shower particles. The two V_1^+-events discussed in detail in Section 8 above have led to the suggestion that these short-lived particles in the lower chamber are hyperons with at least the two alternate modes of decay given by (A) and (B) above. However, if one accepts neither the interpretation of the V_1^+ cases nor the assumption that the charge exchange counterpart of the decay can occur, the evidence presented above still requires the introduction of a short-lived particle with a rather high rate of production. The observed frequency of occurrence and the apparent long lifetime of the much discussed chi meson[9] does not appear to satisfy the requirements imposed by the present data. However, the small number of observed cases of chi mesons, as well as of charged V-particles in this experiment, makesit impossible to exclude completely the possibility that the particles observed in the lower chamber are chi mesons. The particle decaying according to the scheme proposed by Gregory et al.[22], in view of the observed long mean life, is also excluded by the requirements imposed by the present data, although it is quite possible that a few of the events observed in the lower chamber are of this type.

On the other hand, with the acceptance of a charged hyperon as the short-lived particle in the lower chamber, several inferences can be drawn from the data. From the upper limit of the transverse momentum of about 200 Mev/c, the Q-value of the decay scheme (B) can be estimated to be approximately 125 Mev, or less, in agreement with the values reported at the Bagneres Conference[9]

for the hyperons observed in photographic emulsions. The striking similarity of production of these charged hyperons with the neutral hyperons (V_1^o particles) as shown in Table III indicates that they are produced by similar mechanisms. The fact that they are observed with one-third the frequency of the neutral V-particles can in part be attributed to their shorter lifetime and perhaps to a higher energy threshold for production.

The photographic emulsion work indicates that kappa mesons are produced at least as frequently as the hyperons, so that from the curves in Fig. 12 an estimate of the kappa lifetime of the order of 3×10^{-9} sec can be obtained. As seen from the shape of the lower chamber curve, this conclusion is essentially independent of the lifetime and mass of the charged hyperon. Any predominance of kappas over hyperons at production will cause a corresponding increase in the estimate of the kappa lifetime.

In the interpretation of Table II, which gives the charge distributions observed in the two chambers, it ought to be emphasized that the asymmetries indicated by the table are statistically significant only if an explanation in terms of a single type of particle is attempted. If, however, there are several types of charged V-particles separated automatically according to lifetime by the geometry of the two chambers, then a further interpretation of the observed charge distributions as indicating a predominance of one sign of charge or the other at the point of production for each of these types of particles must be undertaken with caution.

10. LIST OF FIGURES

Fig. No.	TITLE	PAGE
1	The arrangement of counters and lead blocks around the cloud chambers.	49
2	Event No. 78113, (listed in Table VIII).	53
3	The distribution of the charged V-particle decay points.	61
4	Frequency distribution of x/D for the upper chamber.	78
5	Frequency distribution of x/D for the lower chamber.	79
6	Plot of the function $S(\tau)$ versus $1/\tau$	81
7	*Plots of the likelihood function for the two* limiting lifetime estimates obtained from the data of the lower chamber.	84
8	Plot of $F(\tau_o) = \int_o^{\tau_o} L(\tau)\, d\tau$ versus τ_o.	84
9	Frequency distribution of the measured masses.	88
10	Frequency distribution of the measured transverse momenta for the lower chamber.	90
11	Frequency distribution of the measured transverse momenta for the upper chamber.	90
12	The frequency of production vs. lifetime for the lower chamber.	95
13	Event No. 41646, showing a charged V-particle originating in an interaction in the lead plate and decaying into a heavy secondary particle.	99

11. REFERENCES

1. G. D. Rochester and C. C. Butler, Nature 160, 855 (1947)
2. Seriff, Leighton, Hsaio, Cowan, and Anderson, Phys. Rev. 78, 290, (1950)
3. R. B. Leighton and S. D. Wanlass, Phys. Rev. 86, 426 (1952)
4. Armenteros, Barker, Butler, Cachon, and York, Phil. Mag. 43, 597 (1952)
5. Astbury, Chippendale, Millar, Newth, Page, Rytz and Sahiar, Phil. Mag. 43, 1283 (1952), 44, 242 (1953)
6. York, Leighton and Björnerud, Phys. Rev. 95, 159 (1954) (This work contains most of the material presented here).
7. Bridge, Courant, De Staebler, and Rossi. Phys. Rev. 91, 1024 (1953)
8. C. O'Ceallaigh, Phil. Mag. 42, 1932 (1951)
9. Report of the Bagneres Conference, 1952 (Unpublished)
10. Lal, Pal, and Peters, Phys. Rev. 92, 438 (1953)
11. Bonetti, Levi-Setli, Panetti, and Tomasini, Nuovo cimento, 10, 1729 (1953)
12. York, Leighton and Björnerud, Phys. Rev. 90, 167 (1953)
13. Anderson, Cowan, Leighton, and van Lint, Phys. Rev. 92 1089 (1953)
14. Leighton, Wanlass, and Anderson, Phys. Rev. 89, 148 (1953)
15. H. A. Bethe, Phys. Rev. 70, 821 (1946)
16. Fowler Shutt, Thorndike, and Whittemore, Phys. Rev. 93 861 (1954)
17. W. L. Alford and R. B. Leighton, Phys. Rev. 90, 622 (1953)
18. M. S. Bartlett, Phil. Mag. 44, 249 (1953)
19. H. Cramer: Mathematical Methods of Statistics, (p. 388) Princeton University Press (1946)
20. C. M. York, Phil. Mag. 43, 985 (1952)
21. Barker, Butler, Sowerby, and York, Phil. Mag. 43, 1201 (1952)

22. Gregory, Lagarrigue, Leprince-Ruiguet, Muller, and Peyrou, Nuovo Cimento 11, 292 (1954)

23. Mezzetti and Keuffel, Phys. Rev. 95, 858 (1954)

24. Kim, Burwell, Huggett, and Thompson, Phys.Rev. (1954) (In press)

25. Leprince-Ruiguet and Rossi, Phys. Rev. 92, 722 (1953) (A summary of experimental evidence)

26. C. F. Powell, Supplemento al Nuovo Cimento 11, 165 (1954) A review article)